Chapter 7
Computational and Experimental Analysis of Carbon Functional Nanomaterials

Pitchaimani Veerakumar, Namasivayam Dhenadhayalan, and King-Chuen Lin

Abstract Density functional theory (DFT) as one of molecular simulation techniques has been widely used to become rapidly a powerful tool for research and technology development for the past three decades. In particular, the DFT-based theoretical and fundamental knowledge have shed light on our understanding of the fundamental surface science, catalysis, sensors, materials science, and biology. Oxygen, nitrogen, boron, phosphorus, and sulfur are the most common heteroatoms introduced on the functional carbon nanomaterials surface with different surface functionalities. This book chapter aims to provide a pedagogical narrative of the DFT and relevant computational methods applied for surface chemistry, homogeneous/heterogeneous catalysis, and the fluorescence-based sensing properties of carbon nanomaterials. We overview several representative case studies associated with energy and chemicals production and discuss relevant principles of computationally driven carbon nanomaterials design.

Keywords Carbon nanomaterials · Density functional theory · Graphene · Catalysis · Sensors · Carbon dots

7.1 Introduction

In recent years, the computational techniques developed for studying the chemical interactions, transformations, and mechanism of the reactions are often based on density functional theory (DFT) [1]. Recent research into the heterogeneous catalysis, a key pathway for the interaction of active metal catalysts in solid supports involving the bond-formation or bond-cleavage reaction or decomposition mechanism, is a subject of considerable debate [2]. This is because of selectivity of

P. Veerakumar · N. Dhenadhayalan · K.-C. Lin (✉)
Department of Chemistry, National Taiwan University, Taipei, Taiwan

Institute of Atomic and Molecular Sciences, Academia Sinica, Taipei, Taiwan
e-mail: kclin@ntu.edu.tw

T. Onishi (ed.), *Theoretical Chemistry for Advanced Nanomaterials*,
https://doi.org/10.1007/978-981-15-0006-0_7

the reaction, tunability of the catalyst, and the choice of solvent toward reactivity and selectivity, etc. which play vital roles in catalysis [3]. The electronic structure calculations by DFT are useful for characterizing the chemical and physical properties of bare and functionalized materials [4, 5]. As such, many graphene-based nanomaterials and related catalysis have been explored and designed with implementation of the classes.

Plane-wave density functional theory (DFT) is a powerful tool for gaining insight into bulk and surface structures at accurate, atomic level. The delocalized nature of the plane-wave basis set hinders the application of many powerful post-computation analysis approaches, many of which rely on localized atom-centered basis sets [6]. Traditionally, this gap has been bridged via projection-based techniques from a plane-wave to atom-centered basis. Many numerical methods have been developed to solve plane-wave DFT. It has been popularly classified as three methods including Gaussian basis set methods, linear-augmented-plane-wave (LAPW) methods, and pseudopotential plane-wave (PSPW) methods. All three methods can be made very accurate and have been capable of predicting structures, frequencies, and energetics for a wide class of compounds [7]. However, the current consensus in the quantum chemistry and condensed matter physics communities reflects that only the first two of these three methods are straightforward to apply for first-row transition metals. It would be beneficial for PSPW methods to work well for these systems, because Gaussian basis set and LAPW methods lack certain capabilities. In particular, PSPW methods can perform ab initio molecular dynamics extremely efficiently and treat unit cells up to a few hundred atoms. Another advantage of PSPW methods is their transferability from molecules to surfaces to solids. In contrast, Gaussian-based methods have different basis set requirements for gas and solid phase applications, complicating the transferability of these methods [8]. Plane-wave DFT calculations were usually performed using commercially available programs such as VASP [9], SIESTA [10], CASTEP [10], ABINIT [11], and Quantum ESPRESSO [12] program packages.

Recently, the modern density functional theory is molecular orbital DFT (like valence bond and molecular orbital theory) as a very efficient additional tool in the arsenal of computational methods rather than a perfectly different theory, which is used orthogonal to traditional approaches [13]. A wave function for a single electron is called a molecular orbital (MO). The MO with spatial and spin coordinates are called spin orbitals and are products of a spatial orbital and a spin function. The lowest unoccupied molecular orbital (LUMO) in DFT has as much meaning in describing electron addition as the highest occupied molecular orbital (HOMO) in describing electron removal [14]. Molecular orbital DFT calculations were performed using Gaussian [15], ADF [16], and TURBOMOLE [17] program packages, to investigate important atomic and molecular properties as well as some selected areas of application.

The DFT results over graphene-based catalysts have been widely used for determining the rate-limiting step [18], active sites [19], adsorption and activation mechanisms [20], activation energy [21], and catalytic pathways [22], which cover almost all catalysis-related topics. Perhaps one of the most illustrious examples

that showcase the development of DFT methodology is a direct non-oxidative conversion of methane to ethylene, aromatics, and H_2 [23]. Obtaining accurate information on the energetics for these processes is challenging. Advanced quantum chemical methods with faster computers are enabling the prediction of accurate energetics of chemical transformations of the larger molecules involved in the processes [24].

The chemical interactions and transformations at the gas-solid, liquid-solid, and gas-liquid interfaces are facilitated by the solid or liquid surface form the basis of the advanced functional catalysis that drives the production of many value-added chemicals [25, 26]. Recently, one approach to circumventing ongoing challenges is through the use of metal-free catalysts as substitutes. Although organocatalysts have been effective in this role [27], carbon-based catalysts derived from graphite, graphene (Gr), or graphene oxides (GO) and other similar materials may serve as useful alternatives [28]. It has been reported that graphene-based catalysts can also work in oxidation of aryl and alkyl alcohols [29, 30], hydrochlorination [31], nitrobenzene reduction [32], and so on. In addition, other applications of graphene materials in catalysis may contain hydrogenation (HYD), hydrodesulfurization (HDS), hydrodenitrogenation (HDN), hydrocracking (HCR), hydrodeoxygenation (HDO), and hydrodechlorination (HDCl). Beyond the exploration of its novel fundamental reactivity, the use of GO as a catalyst is attractive from a practical perspective, owing to the abundance of natural carbon sources, the catalyst's low density, extensive chemical functionalization, hydrophilicity, low cost, and ease for preparation [33]. For deeply understanding the reaction processes, it is strongly suggested to combine DFT computational results with experimental observation. On the other hand, the graphene catalysts co-doped with two or three heteroatoms were also extended [34]. For instance, Zhao et al. reported a universal strategy to synthesize an N-P-O co-doped free-standing three-dimensional (3D) graphene through a one-pot red phosphorus-assisted "cutting-thin" technique [35]. The DFT calculations verified that the enhancement of charge delocalization should be beneficial for the electrochemical applications [36, 37]. We will introduce the DFT computations in this section to rationalize experimental results in graphene-based catalysis, due to their extensive applications when combined with the related characterization techniques [38, 39].

In this chapter, we comprehensively summarized the theoretical chemistry for graphene-based nanomaterials by computation methods covering active surface sites and surface defect structure analysis, binding ability determination, and reaction mechanism investigation. We reviewed the advantages/disadvantages and challenges and further provided key information to catalysis community on how to adopt suitable computation methods for their research. In addition, the electronic and sensing properties of fluorescent carbon nanomaterials are reviewed from a theoretical perspective.

7.2 Density Functional Theory

Density functional theory (DFT) is primarily a theory of the electronic structure of atoms, molecules, and solids in their ground states, in which the electronic density distribution n(r) plays the central role. It is one of the standard computational tools in the condensed matter, chemistry, and biochemistry in both academia and industry [40]. Up to now, the DFT is presently the most successful and also the most promising approach to compute the electronic structure of materials. It provides the description of electronic structure (i.e., structure prediction) and enables to calculate the optical properties, total energies (thermodynamics and kinetics), and forces of materials under very general conditions [41]. The theory was extensively applicable for atoms, molecules, solids, nuclei, and quantum as well as classical fluids [42]. In its original formulation, the DFT provides the electron density which plays a key role in describing the ground state properties of a material. Later on in the field of chemistry, the DFT is employed to predict a great variety of molecular properties including molecular structures, vibrational frequencies, atomization energies, ionization energies, electric and magnetic properties, reaction paths, etc. [43]. The original DFT has been generalized to deal with many different situations: spin-polarized systems, multicomponent systems such as nuclei and electron-hole droplets, free energy at finite temperatures, superconductors with electronic pairing mechanisms, relativistic electrons, time-dependent phenomena and excited states, bosons, molecular dynamics, etc. [44]. For example, the energies of the functional group and the interaction of carbon dioxide were investigated by DFT calculations with the use of the $DMol^3$ code [45] and selection of generalized gradient approximation (GGA-PBE) by Perdew, Burke, and Ernzerhof (PBE) [46]. The atomic orbital was described using double numeric polarization (DNP) basis set, which is comparable to 6-31G (d,p). The van der Waals correction was further taken into account [47]. The type of core processing is set up using a DFT half-core pseudopots (DSPP) specifically designed for $DMol^3$ calculations [48]. The real-space orbital global cutoff radius is 3.7 Å. The convergence threshold parameters for the optimization are 10^{-5} Hartree (energy), 2×10^{-3} Hartree (gradient), and 5×10^{-3} Hartree (displacement) [49].

Since the 1960s, the DFT was introduced in two seminal papers by the authors Hohenberg-Kohn and Kohn-Sham, and its citation is soon up to ~4000 (1964) ~9000 (1965). The annual paper collections dealing with the DFT application are shown in Fig. 7.1 [50]. Note that the relatively small number of publications before 1990 by no means implies that important work was not being carried out. It was a very well-established computational technique, and "density functional" or other designations are named in many applications. Remarkably, the number of publications per year (1975–2014) on topics ("density functional" or "DFT") is listed, according to the Web of Science Core Collection (February 2015). The inset shows data near 1990 on an expanded scale [51]. Obviously, it shows the dramatic increase in the number of publications on the topics "density functional" and density functional theory "(DFT)" in recent years. DFT was promptly incorporated into

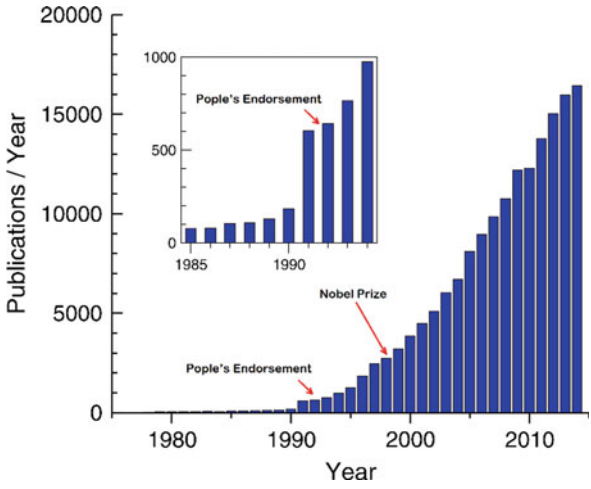

Fig. 7.1 Number of papers that mention DFT as found by the Web of Science. (Reproduced with Ref. [51]. with permission from the American Physical Society)

Pople's widely used Gaussian computer program, and, with this endorsement, the popularity of DFT calculations among chemists began to grow exponentially (see Fig. 7.1). Accordingly, when the Nobel Chemistry Committee decided it was time to honor quantum chemistry with a Prize, it was not difficult for them to split the award between John Pople and Walter Kohn.

7.3 Graphene-Based Functional Nanomaterials

As reported, the pristine graphene (Gr) is a defect-free and stable material composed of a single two-dimensional (2D) layered sheet of polycyclic, hexagonally arranged, sp^2-bonded aromatic carbon [52–54]. However, the production of monolayer graphene may yield by-product of few-layer graphene (FLG) which contains a number of stacked sheets of pristine Gr (usually less than 10). For effective catalytic reactions, fabrication of irregularities and/or defects in the structure of pristine Gr is required. The way to generate irregular structure of pristine Gr was by replacement of some carbon atoms with either sulfur, nitrogen, or other dopants (e.g., phosphorus and boron) [55]. Then, the activity of Gr catalysts was enhanced significantly after dopants were doped on the surface. Figure 7.2a, b show the structures of pristine Gr and heteroatom-doped Gr. As a highly oxidized form of pristine Gr, graphene oxide (GO) is produced by the chemical oxidation of graphite, followed by the exfoliation of single monolayer sheets, and its structure is shown in Fig. 7.2c [56]. The model chemical structural of GO has six-membered benzene rings along with several functionalities such as hydroxyl, carboxyl, epoxy, and ketone, which are represented in different color. Conversely, the aromaticity of the pristine Gr can be partially reestablished by the reduction of GO to yield reduced graphene oxide (RGO) which still contains some residual oxygen as well as the defects both on the

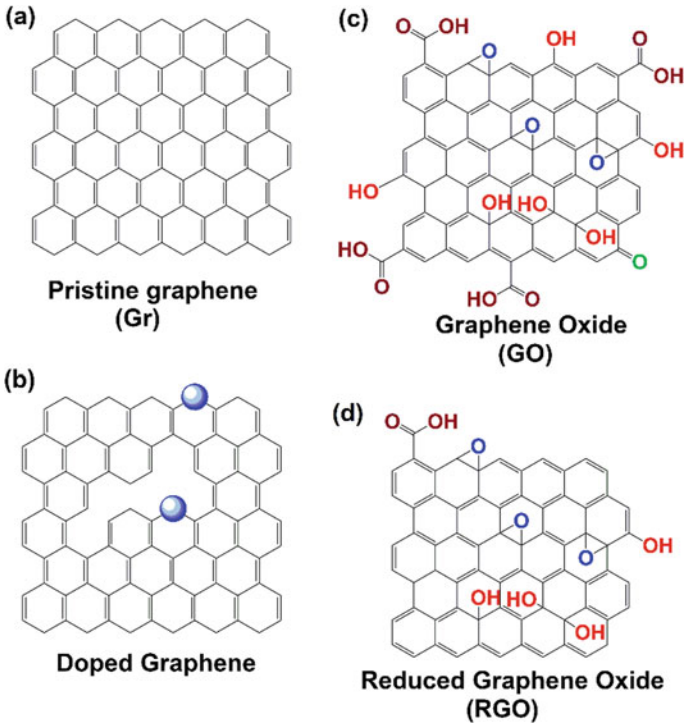

Fig. 7.2 Pristine graphene and graphene-derived solids. (Reproduced from Ref. [52] with permission from the American Chemical Society)

basal plane and at the edges of sheets, as displayed in Fig. 7.2d. The heteroatom-doped graphene or GOs act as catalyst support, in which both the irregularities and residual O-containing groups play a vital role during reaction mechanism in organic transformations and other reactions.

7.3.1 Active Sites of Graphene-Based Metal-Free Catalysts

Generally, graphene-based materials have been widely studied the field of metal-free catalysis due to the outstanding electronic, thermal, and mechanical properties [57]. The unprecedented features of metal-free catalysts, which are believed to account for their superior catalytic performance, have been studied by computation methods. The perfect pure graphene essentially exhibits very low catalytic activities, because of the low density of states around the Fermi level, but it is active at the defects and edges [58]. An effective way is to reduce the lateral size in order to increase the active edges. Nevertheless, in-plane structure of graphene bears a very low chemical activity, which may be apparently enhanced by doping different heteroatoms such

as O, N, B, S, P, and their corresponding functional groups [59]. Catalytic active sites on graphene carbon nanomaterials may be generated by tuning electronic structures. Several approaches are reported. First of all, introducing intrinsic defects and the edge topological structures [60] may facilitate the electron transfer which is beneficial to the conductivity and catalytic activity of carbon nanomaterials. Therefore, to enhance the catalytic activities is probable by optimizing the topology through the charge density analysis on these defective carbon materials by DFT methods. Doping atoms in graphene-based nanomaterials is an alternative approach, based on which carbon atoms are substituted by heteroatoms, such as N, P, and B, or bonded with heteroatoms (O, S, Se, Cl, Br, and I) on carbon surfaces or edges [61]. Such an atomic replacement results in distinct difference of electronegativity, thus leading to localization of, the charge and spin densities and enhancement of the catalytic activities. The active sites are located at the carbon atoms nearby the dopant or at edges, or dopant atom itself. The DFT calculations verified that doping heteroatom (N, O, B, S, Cl, P, Cl, Br, and I) in graphene remarkably changed the charge density and spin density distributions on the doped carbon materials and consequently enhanced their catalytic and electrocatalytic properties [62, 63]. Carboxyl (-COOH), carbonyl (-C=O), and hydroxyl (–C-OH) containing oxygen functional group exhibited the synergistic effect of edge defects on graphene to enhance catalytic activities [64]. The final approach is to physically adsorb organic molecules on graphene or hybrid structure of N-doped graphene [62]. Defects on carbon materials can induce the electron transfer between the organic molecule and the graphene or between the graphitic carbon nitride (g-C_3N_4) and the doped graphene [60]. However, the DFT calculation shows that an electron transfer occurs from graphene sheets to the adsorbed tetracyanoethylene (TCNE) molecules. In addition, the carbon atoms with higher charge density can generate the catalytic active sites due to the electron transfer from the graphene to TCNE molecule [64].

The oxygen functionalities for GO can be introduced via chemical oxidation. These oxygen functionalities with acidic and oxidative nature render GO to function as a solid acid or green oxidant. Besides, the edges or defect sites in GO are found to carry carboxylic acids, quinones, and aromatic CH, as well as the spin electrons. The resulting quinone and diol redox sites play the role as active sites in carbon materials for oxygen-activation reactions. In addition, the amphiphilic character of GO should be advantageous for acting as a phase-transfer catalyst in oil-water biphasic systems [65]. The potential different active sites of graphene scaffold are displayed in Fig. 7.3 [66].

In order to alter the identities of the N moieties, the content of graphitic N species, pyridinic N centers, and pyrrolic N moieties could be tuned through annealing of GO with various N-rich precursors such as ammonia, polyaniline, or polypyrrole, thereby making this process more suitable for practical applications, and the schematic diagram is shown in Fig. 7.4 [67].

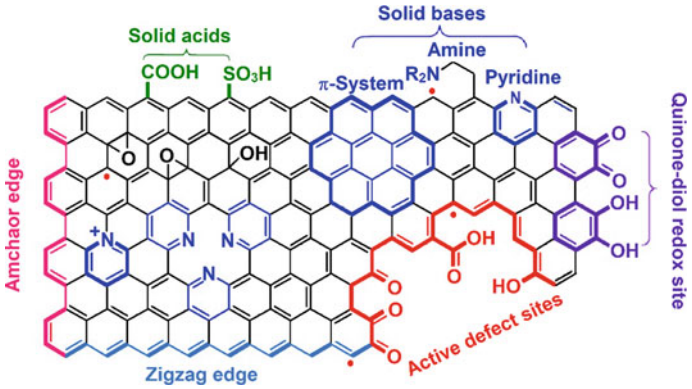

Fig. 7.3 Schematic representation of catalytic active graphene sites on the edges, defects, heteroatoms, and groups. (Reproduced from Ref. [66] with permission of the American Chemical Society)

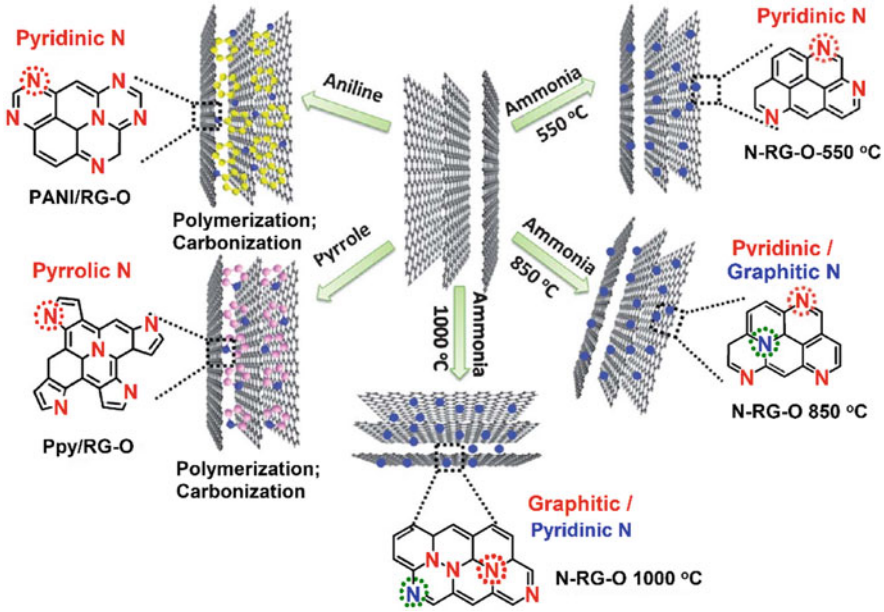

Fig. 7.4 Schematic diagram for the preparation of N-graphene with different N states. (Reproduced from Ref. [67] with permission of the Royal Society Chemistry)

7.3.2 Oxidation Reactions

Currently, the GO with oxygen-containing functional groups is applied to efficiently catalyze the oxidative reactions for value-added chemicals [33, 68]. Therefore, GO can be considered as a green oxidant to oxidize substituted cis-stilbenes to their corresponding diketones [69, 70]. On the other hand, a proton source is necessary

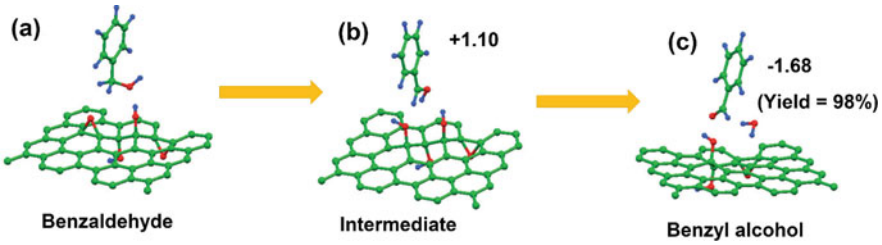

Fig. 7.5 Optimized atomic structures for the (**a**) initial, (**b**) intermediate, and (**c**) final steps of benzyl alcohol oxidation over GO with the initial coverage of epoxy and hydroxyl groups, in which 12.5% of the carbon atoms are on the material's basal plane. The total energy of the reactions is reported in eV. (Reproduced from Ref. [29] with permission of Wiley-VCH)

when GO and RGO are treated as supports for the preparation of bifunctional catalysts. Gomez-Martínez et al. [56] demonstrated that a proton can be generated by the dissociation of sulfonyl groups, i.e., ($-SO_3H \rightarrow SO_3- + H^+$). Although less efficiently, proton can also be donated by carboxylic and hydroxyl groups present on the surface of GO and RGO. The carboxylic acid functionalized GO (GO–CO_2H) few-layers are able to catalyze the pinacol rearrangement and the direct nucleophilic substitution of allylic alcohols. In most cases, GO functionalization is the best way to achieve the performance in oxidation reactions. According to the DFT and experimental results, Boukhvalov et al. [29] have proposed that epoxide functional group may play a role in the metal-free oxidation reactions (Fig. 7.5). For example, benzyl alcohol oxidation (Fig. 7.5a) initiates the reaction, followed by hydrogen transfer from -CH_2 group of benzyl alcohol to GO surface as intermediate (Fig. 7.5b) and terminated with ring opening of epoxide group on the GO surface. This process appears to be energetically favorable pathway. Moreover, the DFT model calculations exhibit the relevant reactivity, mechanisms, and total energies for such an oxidation reaction reported experimentally (Fig. 7.5c).

7.3.3 Oxidative Dehydrogenation

Metal-free graphene shows interesting catalytic properties also in oxidative dehydrogenation (ODH) [71–73], in particular, the selective gas-phase oxidation of acrolein (C_3H_4O) to acrylic acid ($C_3H_4O_2$) [74]. Figure 7.6 displays the reaction mechanism proposed for the oxidation of C_3H_4O on the graphitic carbon surface. Along a rectangular section of a planar graphene sheet with a hole defect illustrates the sp^2 carbon acting as a bifunctional catalyst in the active domain which is terminated by arbitrarily positioned oxygen functionalities. Hence, O_2 adsorbs dissociatively at the (0001) surface to form mobile epoxy groups, feasibly migrating to the prismatic edge sites [75]. The C_3H_4O adsorbed at the nucleophilic oxygen sites, i.e., the ketones/quinones, initiates its oxygenation by epoxy oxygen atoms

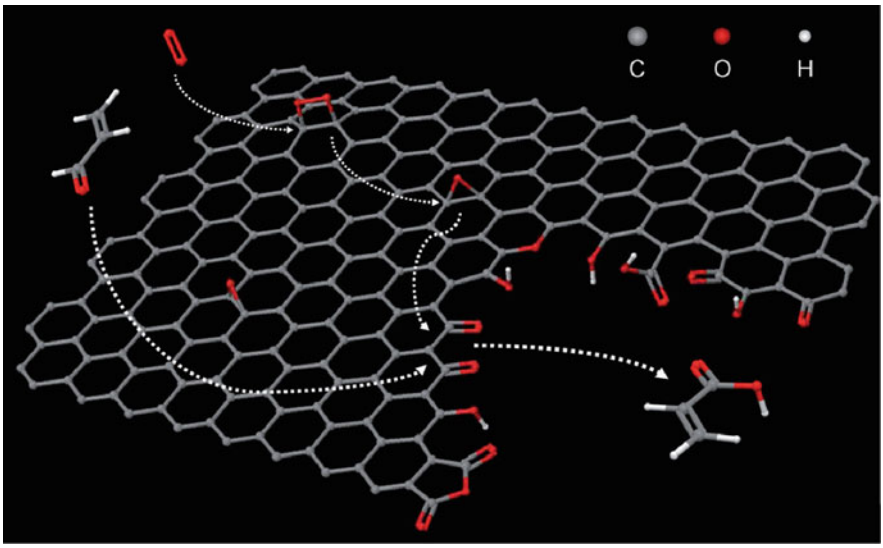

Fig. 7.6 Reaction pathway proposed for the oxidation of C_3H_4O at the graphitic carbon surface. (Reproduced from Ref. [74] with permission of the Wiley-VCH)

to form acrylic acid. Ni et al. [76] showed that graphite-like nitrogen and Stone-Wales defect nitrogen with higher concentration of nitrogen may decrease the dissociation barrier by 0.2 eV more efficiently than pyridine-like nitrogen, due to partial occupation of π_* orbitals and change of work functions.

Tang and Cao [77] showed that the epoxy groups on the GO surface provided active sites around which the -OH groups remarkably enhanced the C–H bond activation of propane (Fig. 7.7). However, high catalyst loading is required for the widespread application of GO in these oxidative reactions. The DFT calculations were performed on the oxidative dehydrogenation of propane over GO. In Fig. 7.7, the pathways denoted by the red and blue lines are associated with two different GO structures including one epoxide group (GO10) and one added to neighboring OH at the opposite side with respect to other oxygen groups on GO10 (GO20), respectively. Figure 7.7 also shows all energies (kcal mol^{-1}) with respect to propane adsorbed onto GO and the optimized configurations (distances in Å) of the initial, transition, and final states.

7.3.4 Friedel-Crafts Reaction

Very recently, a low GO loading has been demonstrated to promote effectively site-selective allylic alkylation of thiophenes with alcohols under mild reaction conditions (Fig. 7.8) [78].

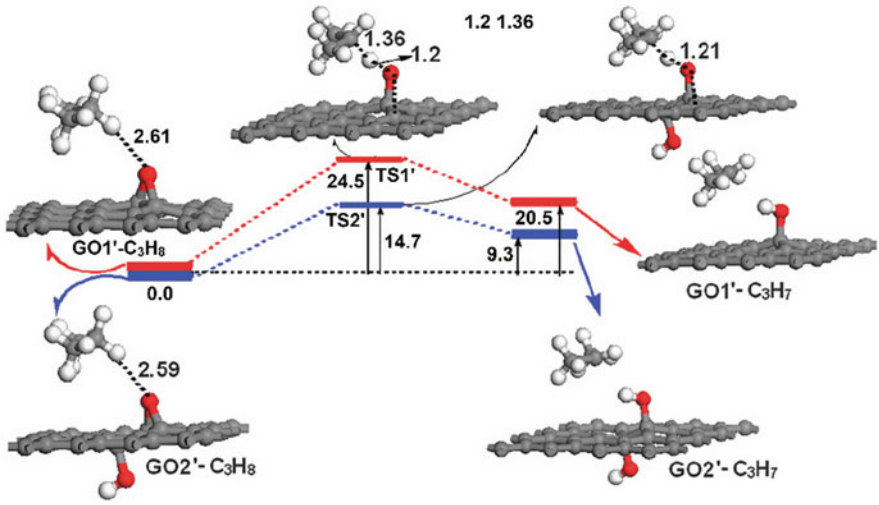

Fig. 7.7 Relative energy profiles for the first H abstraction from CH_2 of propane on GO. (Reproduced from Ref. [77] with permission from the Royal Society of Chemistry)

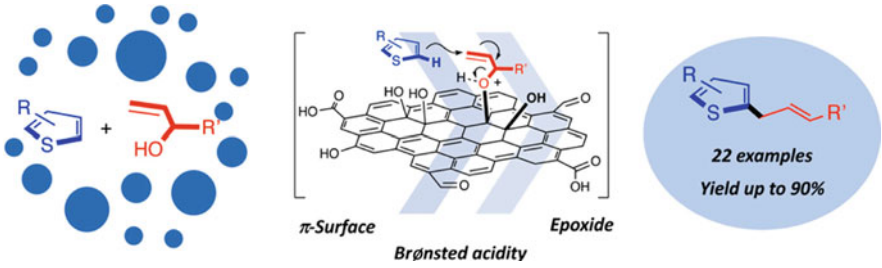

Fig. 7.8 GO-based Friedel-Crafts-type alkylation of alkenes. (Reproduced from Ref. [78] with permission from the American Chemical Society)

The stoichiometric amounts of styrene oxides were carried out intentionally as a control experiment to verify the potential role of the oxiranes moieties present in the GO surface on the reaction mechanism. Such a mechanism justifies the spectroscopic observation by XPS showing the overall increase of alcoholic moieties versus the oxirane ones. The reaction mechanism contains a three-step process, as depicted in Fig. 7.9a. In step 1 the allylic alcohol grafts to the GO surface, followed by an S_N1 mechanism in which the epoxide ring on the GO surface releases a proton to form an unstable oxonium unit that opens without overcoming any barrier ($\mathbf{R_x}$). The proton source could rely on the intrinsic Brønsted acidity of GO. The next step undergoes a reactive α-carbocation in which a nucleophilic attack occurs by the allylic alcohol (**Ts1**). From this picture, the GO π-system plays a crucial role in stabilizing the carbocation generated by the epoxide ring opening event. The compensation effect can be explained probably based on the transition

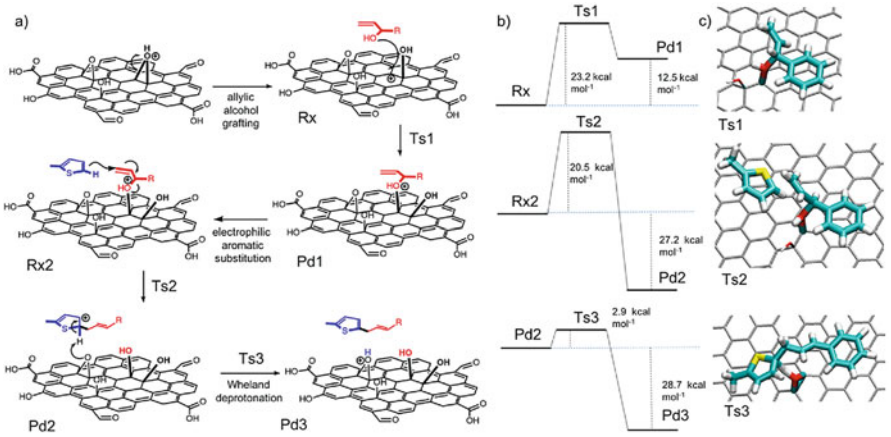

Fig. 7.9 (**a**) Schematic representation of the reaction mechanism; (**b**) energy profiles for the three steps; (**c**) 3D representation of the identified transition states. (Reproduced from Ref. [78] with permission from the American Chemical Society)

state theory of chemical reactions, in which the energy levels are given in Fig. 7.9b. The concerted reaction of the GO π-system and the functional groups present in the 2D-material are marked, consistent with experimental observations. The resulting protonated allyl ether may undergo a Friedel-Crafts-type allylic alkylation yielding the observed allyl-thiophene (**Pd1**). In step 2, a concerted mechanism is followed, showing the α-carbon of the 2-methyl-thiophene attacks the allylic position (**Ts2**), inducing a reorganization of the π-system (Fig. 7.9c). The leaving O−H group remains grafted on the GO surface (**Pd2**). The deprotonation of the Wheland-like intermediate (**Ts3**) is the final step which is a fast process with a calculated barrier of only 2.9 kcal mol^{-1}carried out by other epoxide groups on the GO surface.

7.3.5 Oxidative Coupling

In the chemical catalysis, Loh and coworkers demonstrated this mechanism by the oxidative coupling of amines using porous ba-GO as a metal-free catalyst [79]. The "ba-GO" was denoted, when the base reduction followed by acid reprotonation steps were involved in the preparation of GO under reflux conditions. It was resulted from a sequential base and acid treatment of GO prepared by Hummers' method. Given only 5.0 wt% loading of the carbocatalyst, the imine reached a 98% yield under solvent-free, atmospheric conditions, which is as comparable or even superior to that based on transition metal catalysts. The low catalyst loading is superior to most of the catalysis reaction involving GO catalyst. The dramatically enhanced catalytic activity was contributed to the synergistic effect of the unique functionalities along the edge defects that were created during the base-acid treatment, specifically the

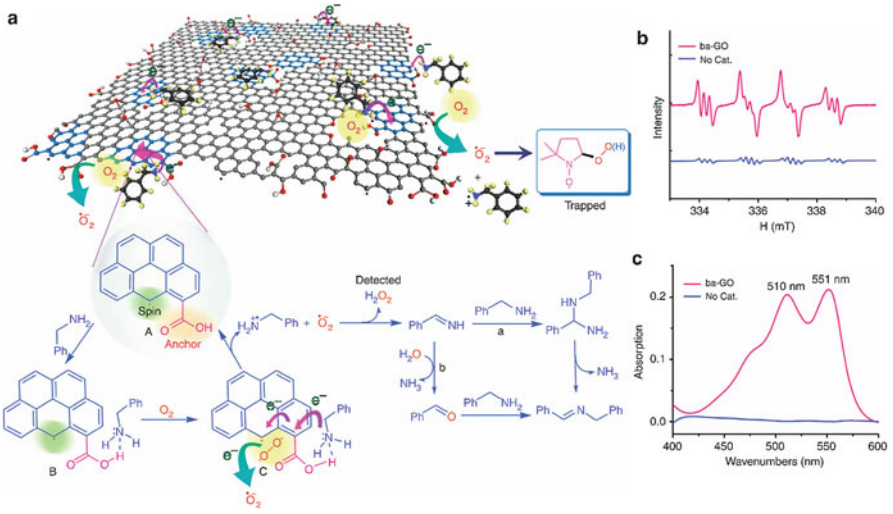

Fig. 7.10 Proposed mechanism of ba-GO-catalyzed oxidative coupling of primary amines. (Reproduced from Ref. [79] with permission of Springer Nature)

unpaired electrons and carboxylic acid (-COOH) groups (Fig. 7.10). The base treatment may generate a large amount of nanoholes and their associated edge defects on the basal planes of GO. These edge sites with unpaired electrons behave as the active catalytic sites which enhance the kinetic rates for the trapping and activating molecular oxygen by a sequence of electron transport and reduction steps to superoxide radical ($\bullet O_2$), which acted as the oxidant in this catalytic reaction. The following three designed experiments supported the proposed hypothesis. Firstly, electron paramagnetic resonance (EPR) is employed to measure the localized spins created at the edge of ba-GO. Secondly, comparable catalytic reaction is carried out to inspect if the catalytic activity decreased upon selectively blocking the unpaired electrons via a diazonium coupling reaction. Finally, in situ spin-trapping EPR experiment is conducted to trap the in situ formed radicals. The carboxyl anionic groups can be obtained by the acid treatment to position along the edges to carboxylic acid groups, which produced a synergistic effect for the coupling reaction. These carboxylic groups may act as hydrogen bonding sites to the amines and facilitate proton transfer reactions due to acidic properties. Further, the base reduction eliminated the hydroxyl groups from the GO and thus changed the dynamics of water solvation layer around GO, allowing more amount of reactants into the catalytic sites. The solvent-free and metal-free catalysis with low catalyst loading is an ideal model for practical application such as industrial-relevant carbocatalysts. The RGO as metal-free catalysts were also demonstrated in oxidative desulfurization reactions using molecular oxygen as the terminal oxidant [80].

The RGO catalyst was demonstrated to be capable of effectively removing a broad range of sulfur-containing compounds from fuels with excellent reusability. The studies on X-ray photoelectron spectroscopy (XPS), chemical titration method, and a series of comparative experiments revealed that carbonyl groups played a crucial role during the oxidation process. The RGO with defects in such as vacancies is beneficial to the catalytic performance because carbonyl groups could be generated in situ on these defects under the reaction conditions. Although the carbonyl groups were not directly involved in the generation of ROS, their electron-withdrawing properties reduce the electron population of the carbon atoms at their adjacent positions, which facilitates absorption and activation of molecular oxygen. The strongly adsorbed oxygen molecules may then convert to super-oxygen anion radicals (RGO–OO–•). Meanwhile, the sulfur-containing substrates turn into sulfur-centered cation radicals, which react with the negative charged radicals of RGO–OO–• to generate sulfones as the final products.

7.3.6 C–H Bond Activation

Transition metals and organometallic complexes were employed traditionally to catalyze the C−H bond activation [81]. Recently, cheap metal-free catalysts have emerged as promising candidates for this transformation. Gao and coworkers reported that N-doped Gr plays a major role in the work on sp^2 C−H activation that covers the selectivity for the oxidation of arylalkanes in aqueous phase, affording high value-added products for biomedical applications [82]. The N-doped sp^2 hybridized carbon was prepared through a chemical vapor deposition (CVD) process with acetonitrile vapor as the N source with 8.9% N content. DFT calculation suggested that the nitrogen atoms are not able to host the peroxide species because of the high negative charge of nitrogen. Both the electronic charge and spin density on the *o*-carbons are superior positions for the adsorption of reactive oxygen species such as peroxide. Both C K-edge and N K-edge X-ray absorption spectroscopy (XAS) were used to study N-doped carbon catalysts before and after TBHP (*t*-BuOOH) and ethylbenzene treatment, clearly revealing that the graphitic nitrogen dopant modulated the electronic structure of sp^2 carbon material. The intensities of density of states near the Fermi level for the adjacent ortho-carbon are much stronger than those of undoped graphene carbon, which gives the nitrogen-neighboring carbon a metal-like d-band electronic structure.

In 2016, an inexpensive, metal-free GO catalyst used for the C–H bond arylation of benzene enables the formation of bi-aryl compounds in the presence of aryl iodides [83]. The oxygen functional groups in these GO sheets and the addition of KOtBu are essential for the observed catalytic activity. The DFT calculations on reactions with various model compounds confirmed that these negatively charged oxygen atoms promote the overall transformation by stabilizing and activating K^+ ions, which in turn facilitate the activation of the C-I bond, [as benzyl alcohol was a particularly active model system]. Based on DFT calculations, a GO nanopore was

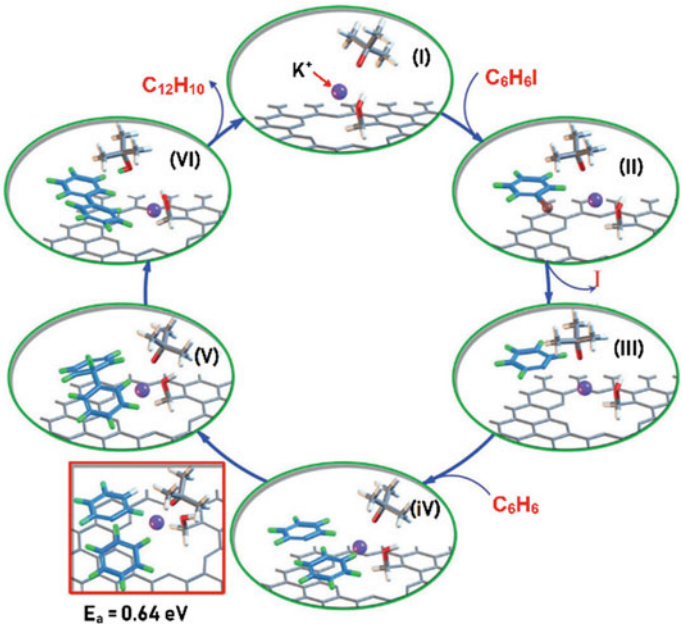

Fig. 7.11 Mechanism proposed for the GO-catalyzed arylation reaction. (Reproduced from Ref. [83] with permission of the Wiley-VCH)

focused (the edge of graphene; Fig. 7.11). The interaction between KOtBu and Gr is very weak without hydroxy groups. Instead, as shown in Fig. 7.11, K^+ can strongly interact with oxygen species at the edge of a Gr nanopore (**I**; the adsorption energy, E_{ad}, is −0.96 eV). The distance between a K^+ ion and the oxygen atom of an ether OtBu moiety is 2.53 Å, whereas the distance between K^+ and a hydroxy oxygen atom is 2.57 Å. At the same time, the π-π interactions between the π system of Gr and that of iodobenzene (C_6H_5I) enable the adsorption of the latter on the same graphene surface (**II**, $E_{ad} = -0.97$ eV) [84]. The charge of the immobilized K^+ ion is 0.89 eV owing to the electron transfer between K and the oxygen group, which is beneficial to the subsequent activation of C_6H_5I. Indeed, the iodine-carbon bond of C_6H_5I can be easily activated by attack of a K^+ ion, which leads to the formation of a C_6H_5 radical. The benzene radical is stabilized by the π system of Gr and the positively charged hydrogen atoms (**III**; $E_{ad} = -1.29$ eV). This intermediate then reacts with adsorbed benzene (**IV**; $E_{ad} = -0.76$ eV) with a moderate activation energy (0.64 eV). After proton transfer, biphenyl is formed (VI). In addition, the Gr π system also greatly facilitates the overall reaction as the aromatic coupling partners are adsorbed.

7.3.7 *Reduction of Nitro Compounds*

Nitroaromatic compounds (NACs) are widely utilized as pesticides, explosives, and synthesis intermediates, [85, 86] causing environmental pollution. The electron-withdrawing effect of the nitro groups and the stability of the benzene ring lead to the recalcitrance of the NACs through either chemical reduction [87] or oxidative degradation [88]. Pal et al. found that 4-nitrophenol (Nip) may be reduced to 4-aminophenol (Amp) by sodium borohydride ($NaBH_4$) in the presence of N-doped graphene (NG), in which the N-doping greatly enhanced catalytic activity [89]. The activity was related to the surface area of the catalysts. Recently, Kong group [90] reported the NG synthesis and its catalytic behavior in the reduction of Nip to Amp (Fig. 7.12a). The catalytic procedure of this reaction was described in Fig. 7.12b. Nip ions adsorb initially on the active sites of NG in solution, and then the adsorbed Nip ions can desorb into water to reach equilibrium. There are a limited number of active sites such that only the carbon atoms next to the doped N atoms can be activated. The adsorption of Nip ions is much faster than its desorption ($k_1 >> k_2$), so that the number of Nip ions absorbed on NG sheets is not determined by their concentration, but by the number of active sites on NG, which will lead to the pseudo-zero-order reaction. The desorption rate of Amp k_4 is very fast during the course of reaction. In contrast, the active sites in metallic catalysts are abundant, and the adsorption rate and desorption rate are comparable so that the amount of adsorbed Nip ions are highly dependent on their concentration, which could lead to pseudo-first-order reaction.

The DFT calculations have also been performed to simulate the adsorption configuration of Nip ion on this metal-free catalyst according to the XPS and in

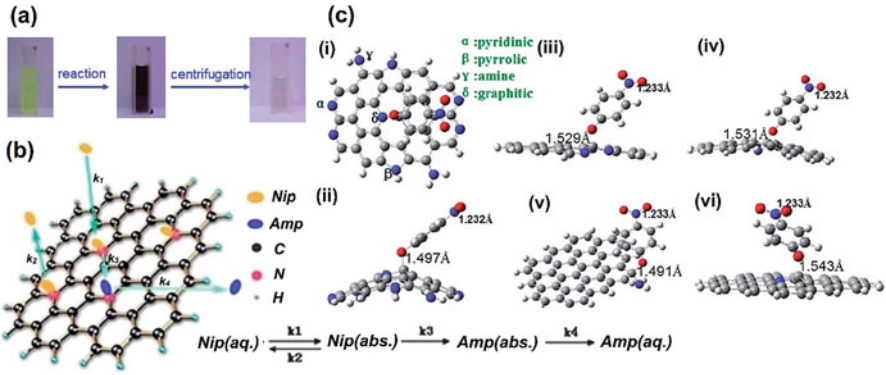

Fig. 7.12 (**a**) Optical photos of the color change during the reaction, (**b**) catalytic process of the reduction of Nip on the surface of NG, and (**c**) the optimized structures of Nip ions adsorbed on NG: (*i*) top view and (*ii*) side view; Nip ions adsorbed at the (*iii*) pyridinic, (*iv*) pyrrolic, (*v*) amine, and (*vi*) graphitic NG. The separated distances and the N–O bond length of nitro group for each model have been marked directly in the corresponding figures. (Reproduced from Ref. [90] with permission of the Royal Society of Chemistry)

situ FTIR results. Only the carbon atom near the doped N atom could be activated to catch Nip ions owing to its weaker conjugation compared to the other carbon atoms. It reflects that the number of active sites on the Gr surface was much smaller than those of metallic nanoparticles. Therefore, the adsorption process of Nip ions on the surface of NG, appearing a different reaction kinetics, was more pivotal than in the cases of metals. Furthermore, the active sites of NG were positively charged owing to the large electronegativity of doped N atoms, so that Nip ions preferred to combine with Gr sheet via the hydroxyl group. Based on the Mulliken analysis, it had a charge of −0.450 electrons, more negatively charged than the −0.246 electrons of the -NO_2 group. This was in agreement with the decrease of O–H vibration of the in situ FTIR results. Interestingly, the XPS data show that there are four kinds of N atoms with a ratio of 4 (pyridinic):2 (pyrrolic):2 (amine):1 (graphitic) acting as the catalytic active site as shown in Fig. 7.12c(i). The NG sheet shows intense distortions, and the Nip ion could combine with the carbon atom (next to the doped N atom) of the NG tightly, with the C–O bond distance at 1.497 Å (Fig. 7.12c(ii)). Together with the strong adsorption energy as mentioned above, it is concluded that the N-doping can indeed improve the adsorption ability of NG, which will contribute to the catalytic properties. The graphitic N atom is at the center of the surface while the others are at the edge. As such, the adsorption of Nip ions both at the center and edge should be considered. Each kind of these doped N atoms was calculated individually, and the results are illustrated in Fig. 7.12c(iii–vi). As expected, every configuration induces strong adsorption of the Nip ions onto NG, showing significantly enhanced adsorption energies with their small separated distances at the interface ca. 1.5 Å. The N–O bond lengths of the nitro group have also been calculated and marked in Fig. 7.12. Moreover, only the carbon atoms next to the doped N atoms on NG surface can be activated, serving as the active sites. As expected, all four kinds of the doped N atoms are beneficial to the adsorption and activation of Nip, contributing to the catalytic reduction reaction.

Li et al. recently reported that reduced graphene oxide (RGO) mediates the reductive transformation of biological NACs by electrochemically active bacteria, such as *Escherichia*, *Desulfovibrio*, and *Enterobacter*, which had been detected in both sludge and sludge-RGO systems [91]. The reduction of nitrobenzene (NB) results shows that RGO could increase the rate by an approximate onefold by mixed culture with glucose (electron donor). The influence of the surface properties of RGO on biological NACs removal was further elucidated. When RGO was used as metal-free catalyst with limited oxygen moieties on the surface of RGO such as quinone groups, the NB transformation rate was decreased, whereas nitrogen-doped RGO framework exhibited a positive effect as well as enhanced reduction rate. Indeed, RGO can absorb NB and form π-π interactions with aromatic rings, which resulted in the electron transfer to NB. Additionally, RGO could mediate direct interspecies electron transfer (DIET) and activate NB molecules. In recent years, it was suggested that DIET is an alternative mechanism for electron exchange through biological electrical connections [92], in contrast to interspecies hydrogen/formate electron transfer. Liu et al. reported that activated carbon promoted DIET [93]. RGO was also expected to accelerate DIET between microbes, which might be favorable

for nitroreductase to accept electrons. Here, RGO plays the role of "extended nanowire." The activation of NB by Gr has been proposed using DFT calculations, and the unsaturated carbon atoms at the edges of Gr and defects on Gr might possess catalytic activity [87].

7.4 Porous Carbon-Based Functional Nanomaterials

Porous carbon materials including traditional activated carbons (ACs), carbon nanotubes (CNTs), ordered mesoporous carbon (OMCs), carbon black (CBs), nanofibers (NFs), and recently emerged novel structured carbons synthesized by hard and soft templating methods have been widely used in a variety of applications [94]. Due to their high specific surface areas, micro−/mesoporous structure, tunable pore size, electronic conductivity, excellent accessibility to active sites, enhanced mass transport and diffusion. These properties make them a special and unique choice for various applications in divergent fields such as energy storage, fuel cells, adsorption/separation, heterogeneous catalysts, catalyst supports, photocatalysis, CO_2 capture, electrochemical sensors, and so forth [95–97]. However, to improve their catalytic properties, surface modification, heteroatom doping, chemical activation, and defects on graphic layers are necessary and have been extensively investigated [98–100]. It is well known that various surface groups, impurities and surface irregularities (i.e., surface heterogeneity), as well as fine pores of different sizes and shapes (i.e., structural heterogeneity) will contribute to the reaction mechanisms. An uneven distribution of functional groups creates surface heterogeneity. Another reason for heterogeneity is the presence of heteroatoms (commonly O, N, and S). However, the emission resulting from graphene has been attributed to C-oxygen-, C-nitrogen-, and/or C-sulfur-related localized states [101]. To induce ripples on the graphene surface can probably alter the local electrical and optical properties of graphene; thus, modified ripple engineering can be used for various applications [102]. Among the elements of complexity are the high surface area resulting from an intricate pore structure, significant differences in the physicochemical parameters among the heterogeneous surface sites, the occurrence of partial delocalization of the π-electrons, and the ability of certain surface sites to react with water and other solvents [103]. Some authors suggest that the distribution of the functional groups on the surface of ACs depends on pore size. The surface area is characterized among microporous materials (<2 nm), mesoporous materials with pore diameter between 2 and 50 nm, and nonporous or macroporous materials with pore diameter >50 nm [104]. The surface reactions of carbon nanomaterials are generally initiated from reactions of C atoms at the edges of the layers or at other lattice defects or reactions of functional groups that are bound to such C atoms. Surface reactions based on carbon as metal-free catalysts are of particular interest. The catalytic performance is significantly increased with an increase in the number of surface oxygen groups present, which are responsible for the enhancement in reaction rate, higher catalytic performance, and yield of the products [105]. Metal-

organic frame work (MOF)-derived ACs, as the other major form of porous carbon, are primarily made of graphitic sheets with regular order and possess extremely high surface areas and large pore volumes which make them extremely promising candidates for applications such as catalyst supports and adsorbents. Due to the presence of favorable pore geometries and volumes, ACs have been used in the areas of gas separation and storage, water purification, electrochemistry, and catalysis [106].

The catalytic behavior of carbon materials depends on their surface properties and unsaturated carbon atoms at the edges of the graphene layers and in basal plane defects that can easily react with oxygen, water, or nitrogen compounds, originating surface groups such as those represented schematically in Fig. 7.13 [107].

These functional groups can be used to metal-free catalysts or catalyst precursors or for subsequent functionalization and so on. In addition, they may be active sites for specific catalytic reactions [108]. Among the oxygenated groups, carboxylic acids and anhydrides, lactones, lactols, and phenols are acidic, while carbonyl and ether groups are neutral or may form basic structures (quinone, chromene, and pyrone groups). The carbon π electrons in the basal planes also contribute to the basicity of the carbon material, affecting its adsorption and catalytic properties [109].

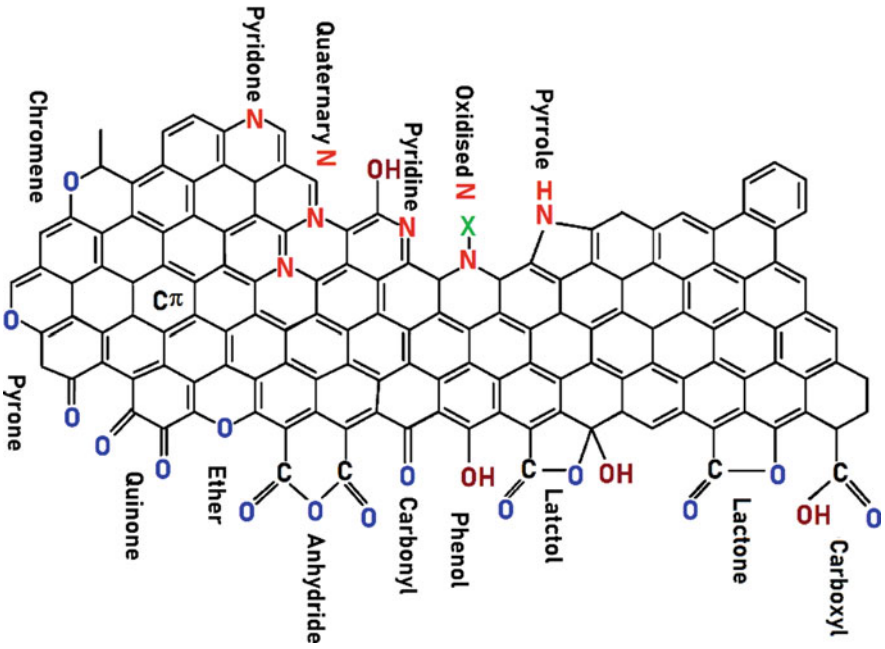

Fig. 7.13 Surface groups on carbon layers. (Reproduced from Ref. [107] with permission of Elsevier)

Recently, PCs have long been used as catalysts in organic transformations such as oxidation phenol [110], ODH of ethylbenzene [111], and anaerobic biotransformation of nitroanilines [112]. But the considerable modification in the porous structure of bare carbon materials, as well as the possibility of chemical and structural changes, offers new opportunities to use the PC materials in many different chemical reactions [113].

Carbon gels (CGs) are obtained by carbonization of organic gels produced by the sol-gel polycondensation of organic monomers such as resorcinol and formaldehyde, as first described by Pekala [114]. It exhibits high porosity and surface area, narrow pore size distributions, and randomly oriented pores, which have been reported as catalysts for quite a large variety of reactions. For instance, CGs functionalized with sulfonic acid groups are active acid catalysts for the esterification of acetic acid with ethanol [115]; N-doped carbon xerogels were used for oxidation of NO [116] and in the degradation of organic pollutants by advanced oxidation processes [117].

Black carbons (BCs) are carbonaceous materials composed of single and stacked polyaromatic sheets in a highly disordered arrangement. These sheets can be functionalized along the edges with hydroxyl (-OH), carboxyl (-COOH), keto (>C=O), or other functional groups. The textural properties such as surface area, pore volume, and pore size were dependent on the source material and conditions of synthesis [118]. It consists of spherical graphite particles (less than 50 nm diameter) with 0.35 nm interplanar spacing. The N_2 gas adsorption measurements reveal high surface area (typically, more than 50 $m^2\ g^{-1}$), high porosity (0.1–0.2 $cm^3\ g^{-1}$), and small pore size, i.e., below approximately 20 Å, with small porosity in the range 4–10 Å. They are most commonly used catalyst support in various environmental applications due to its high surface area (250 $m^2\ g^{-1}$) and low cost [119].

Recent studies have demonstrated that black carbons (BCs) could significantly accelerate the abiotic reduction of NACs in the presence of reductants, after their strong sorption to the NACs [120, 121]. It is well known that the pathway of NB reduction involves three successive two-electron transfer and protonation steps [122].

$$\mathrm{Ar\text{-}NO_2} \xrightarrow[-H_2O]{2e^- 2H^+} \mathrm{Ar\text{-}NO} \xrightarrow{2e^- 2H^+} \mathrm{Ar\text{-}NHOH} \xrightarrow[-H_2O]{2e^- 2H^+} \mathrm{Ar\text{-}NH_2}$$

In addition, the DFT method was applied to calculate the sequences of electron and proton (H^+) for the reduction of NB to aniline [123]. However, the reductions of trifluralin (TF) and pendimethalin (PDM) seem to be more complex with competing reduction pathways, because there are two nitro groups on the benzene rings. Gong et al. reported the results combining the quantum-mechanical DFT calculation with experimental findings to elucidate the abiotic reduction mechanism of two nitro groups in TF and PDM [124]. They displayed the most plausible pathways and calculated energy profiles for reduction of TF and PDM in Figs. 7.14a and 7.15a, respectively.

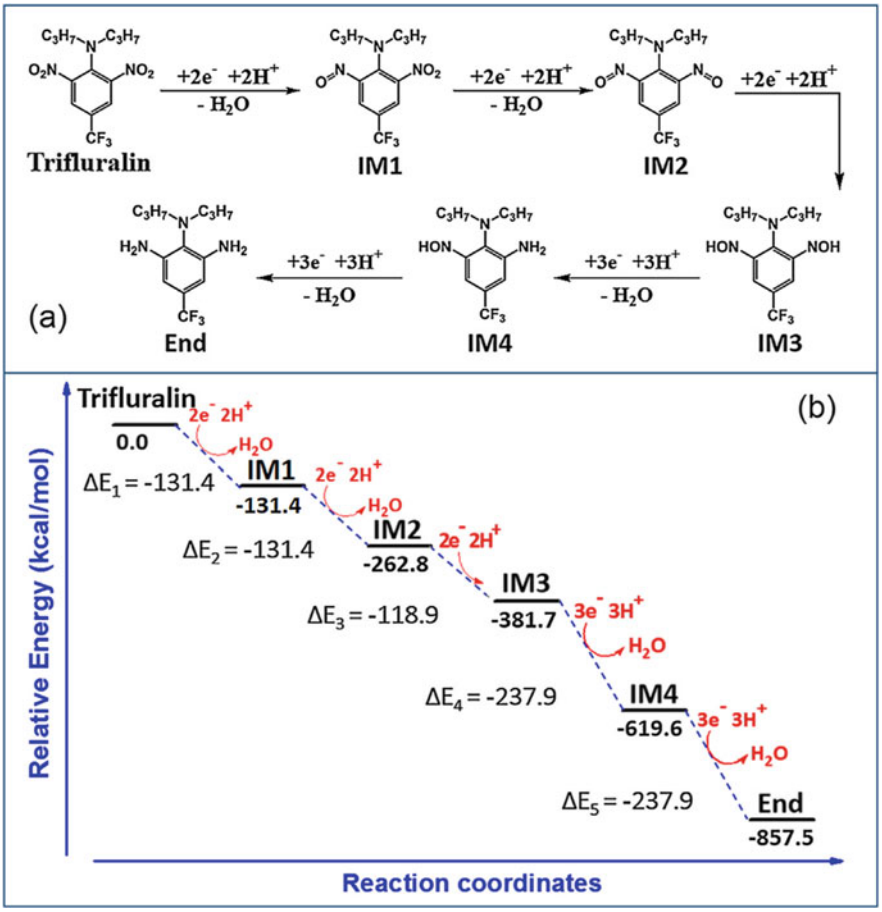

Fig. 7.14 Schematic representation (**a**) and calculated relative energy profiles (**b**) for abiotic reduction of TF. (Reproduced from Ref. [123] with permission of Elsevier)

While inspecting the energy profiles, the reduction of TF and PDM to their corresponding 2-NH_2 products is thermodynamically favorable, because the ΔE value of each step is negative (Figs.7.14b and 7.15b). The reduction intermediates and end products were identified, and the mass spectrum matched the results of detected species. It was noted that not all of the intermediates could be identified probably due to their instability. However, we can find evidence from the calculated quantum chemical properties of the reactants and transformation products. Thus, BCs could promote the abiotic reduction of TF and PDM by sulfides in the anoxic sediments, plausibly by accelerating the transfer of electron and atomic hydrogen from sulfides to dinitroaniline herbicides [124].

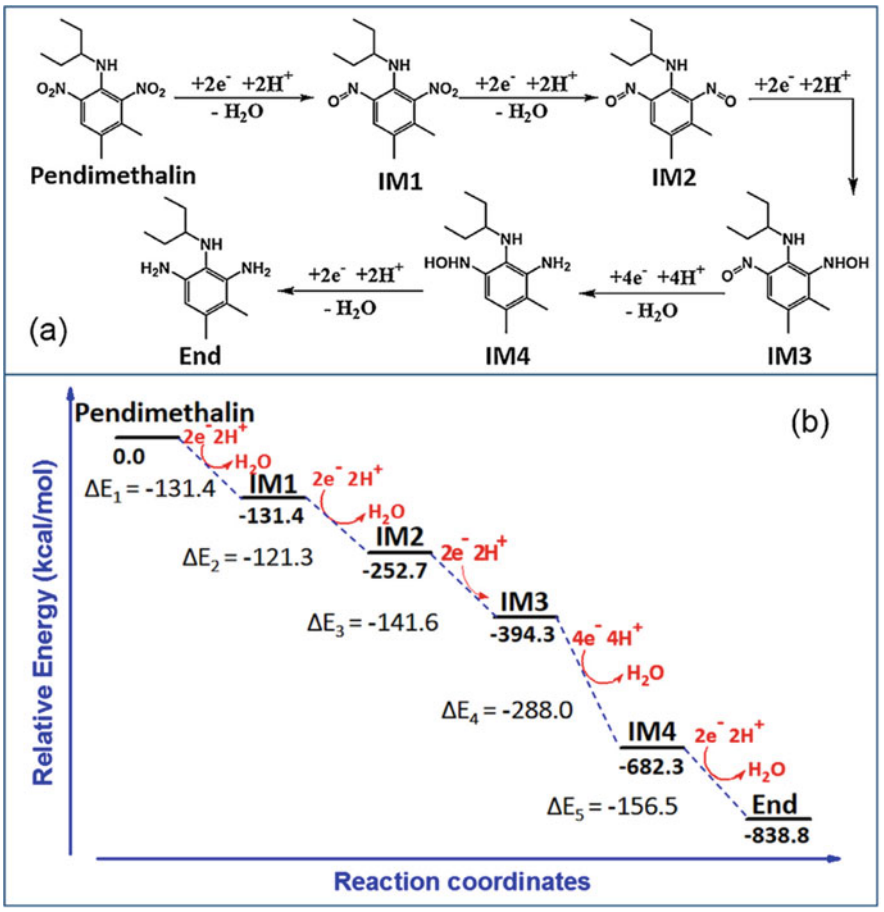

Fig. 7.15 Schematic representation (**a**) calculated relative energy profiles, and (**b**) for abiotic reduction of PDM. (Reproduced from Ref. [123] with permission from of Elsevier)

7.5 DFT Analysis for Structural, Fluorescence, and Sensing Properties of Fluorescent Carbon Nanomaterials

Carbon nanomaterials are one of the emergent advanced nanomaterials, due to their unique physicochemical properties, thereby showing promising performance in diverse applications [125–128]. These appeared in different structures including carbon nanotubes (CNTs), carbon dots (C-dots), graphene, graphene quantum dots (GQDs), graphene oxide (GO), fullerene, carbon nanohorns (CNHs), and carbon nano-onions (CNOs) which have been explored for potential applications in the field of chemistry and biology (Fig. 7.16) [125–128]. The carbon nanomaterials are mainly classified based on their dimensions such as zero-dimensional (0D),

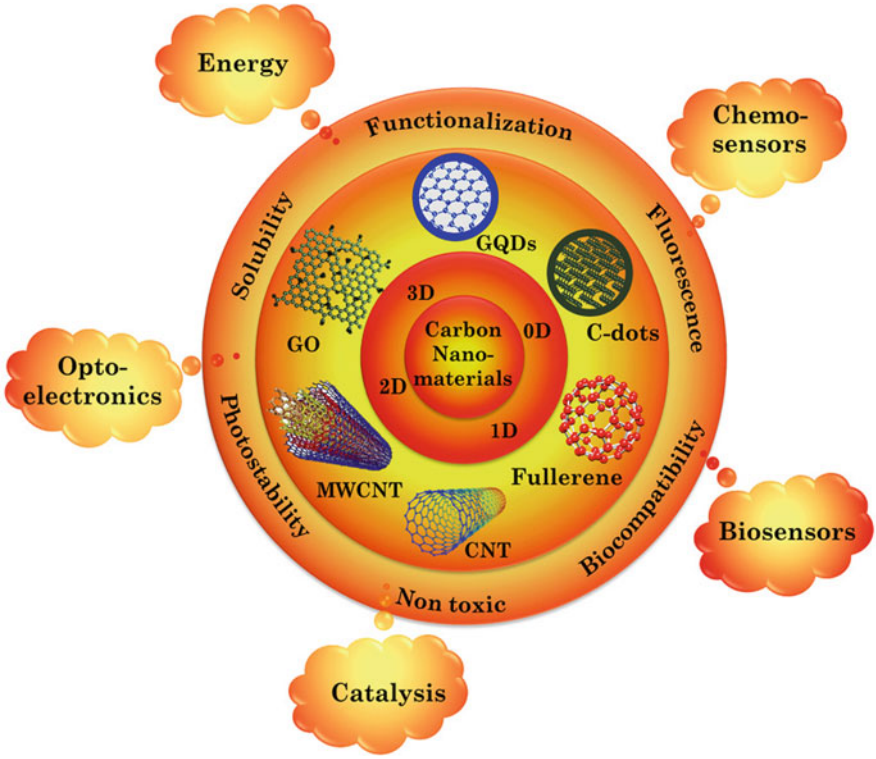

Fig. 7.16 Schematic representation of carbon nanomaterials

one-dimensional (1D), two-dimensional (2D), and three-dimensional (3D) nanostructures. The 0D materials have no dimensions with nanosize range which is considered as a spherical in shape including C-dots, fullerene, and GQDs. The 1D materials (CNTs) have one dimension outside of nanomateric size range (1–100 nm), whereas 2D materials (graphene and GO) possess two dimension lying in a nanosize. Generally, the bulk materials are known to be 3D materials which are composed of individual blocks with the size of nanometer scale (1–100 nm) or more. The 3D materials such as diamond and graphite have all dimensions in macroscale. This dimension-based classification is greatly dependent on the electron movement along the dimensions in the nanomaterials. For instance, electrons in 0D materials are entrapped in a dimensionless space, while electrons move along the x-axis in 1D materials. Similarly, 2D and 3D materials have electron movement along the x-y-axis and x-, y-, and z-axes, respectively. The 0D nanomaterials possess well-defined and quantized energy levels compared to those of other dimensional materials. Because the electron mobility is confined in 0D nanomaterials, the motion of randomly moving electrons is restricted to specific energy levels resulting in the increase of band gap of materials.

Diamond consists of sp^3-hybridized carbons, where the purely covalent chemical bonds extend three-dimensionally. Diamond is known as an electrically insulator due to lack of π electrons. On the other hand, the graphene is a 2D single layer of graphite and known to be very strong conductive material, because the graphene consists of sp^2 bonds. Structurally, a graphene sheet is a single layer of carbon atoms packed into 2D honeycomb lattice structure, whereas the CNTs are considered as rolled-up graphene sheet and their edges of the sheet joint together to form a seamless cylinder. In the case of 0D nanomaterials, GQDS are formed by the cutting a graphene monolayer into the small spherical molecules with the size of below 20 nm. These GQDS are mainly composed of sp^2 hybridized carbon atoms and crystalline in nature. In contrast, the C-dots composed of sp^3 hybridized carbon atoms predominantly with the various combinations of graphitic and turbostratic carbons. Moreover, the C-dots exhibit amorphous nature of their carbogenic cores. Recently, the C-dots and GQDs are getting much popularity among the 1D and 2D carbon nanomaterials. They can be synthesized from diverse kind of carbon precursors including organic molecules (citric acid, carbohydrates derivatives, etc.) and biomolecules (proteins, amino acids, etc.) with facile method and in shorter time. Another important feature is that C-dots and GQDs have photoluminescence property inherently as well as they can be tuned by chemical surface functionalization.

The applications as fluorescence sensors have been extensively studied by using these carbon nanomaterials due to their inherent fluorescence properties and non-toxicity. Among these nanocarbons, the single- and two-dimensional (1D and 2D) materials such as CNTs, graphene, and GO were served as sensing platform. The zero-dimensional (0D) materials like GQDs and C-dots are emerging as promising fluorescence sensing probe in consequence of several unique features including strong fluorescence with tunability, high photostability, smaller in size, ease to be functionalized, biocompatibility, and non-toxicity. Due to these advantages, the GQDs and C-dots materials were widely utilized as a fluorescent sensing probe in chemical and biosensors. The most important feature is that these materials exhibit non/less-toxicity in nature which enhances the potential in their sensor application.

7.5.1 Structural and Fluorescence Analysis of Graphene Quantum Dots and Carbon Dots

Firstly, Suda et al. have prepared the nanometer-size carbon particles on a Si substrate using plasma-assisted pulsed laser deposition (PLD) method [129]. The prepared carbon nanoparticles were in an amorphous state with sp^3 and sp^2 carbon components. Then in 2006, Sun et al. reported the photoluminescence carbon nanoparticles which were then named as “carbon dots” [130]. They observed strong excitation wavelength-dependent fluorescence (Fig. 7.17) which is ascribed to the emissive surface defects caused by the surface passivation of C-dots with organic molecules such as diamine-terminated oligomeric poly-(ethylene glycol)

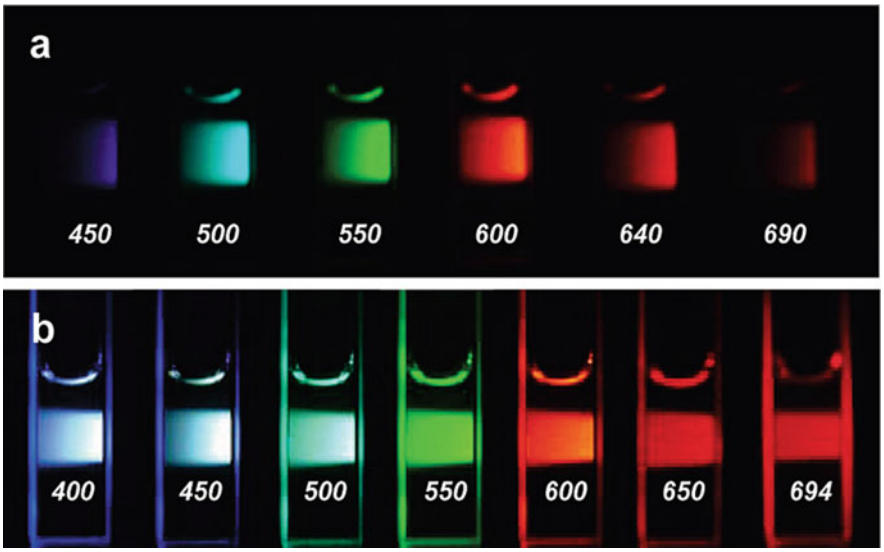

Fig. 7.17 Aqueous solution of the PEG_{1500N}-attached carbon dots (**a**) excited at 400 nm and photographed through band-pass filters of various wavelengths and (**b**) excited at the indicated wavelengths and photographed directly. (Reproduced from Ref. [130] with permission of the American Chemical Society)

(PEG_{1500N}) and poly(propionylethyleneimine-*co*-ethyleneimine) (PPEI-EI). On the other hand, Pan et al. in 2010 first synthesized the fluorescent functionalized GQDs from graphene sheets using hydrothermal method [131]. They have proposed that the luminescence originates from free zigzag sites with a carbene-like triplet ground state described as $\sigma^1\pi^1$. Recently, many research groups have extensively studied the fluorescence properties of C-dots and GQDs and proposed the mechanisms for multi-emissions by experimental observations [132–137]. However, the mechanisms are still not completely understood, because fluorescence properties are highly sensitive to several factors including size and shape of particles, carbon precursor, heteroatom doping, nature of the capping agent, experimental conditions, defects sites, etc. With the aid of theoretical calculations and modelling which provide precise details about the fluorescence properties of C-dots and GQDs, it becomes possible to investigate the influence of each abovementioned factor on the fluorescence properties of materials.

Time-dependent density functional theory (TDDFT) for response properties and excited states, which is a prerequisite to compute electronic spectra and related quantities like dispersion effects on polarizabilities and optical rotation [138–140]. Initially, SK et al. have demonstrated the systematic theoretical investigations of tunable photoluminescence properties of GQDs by regulating its size, shape, edge configuration, functional groups, and defects by using DFT and TDDFT calculations (Gaussian 09 package, B3LYP/6-31G(d) level) [141]. As shown in Fig. 7.18a, the emission wavelengths were linearly dependent on the increasing size of the GQDs,

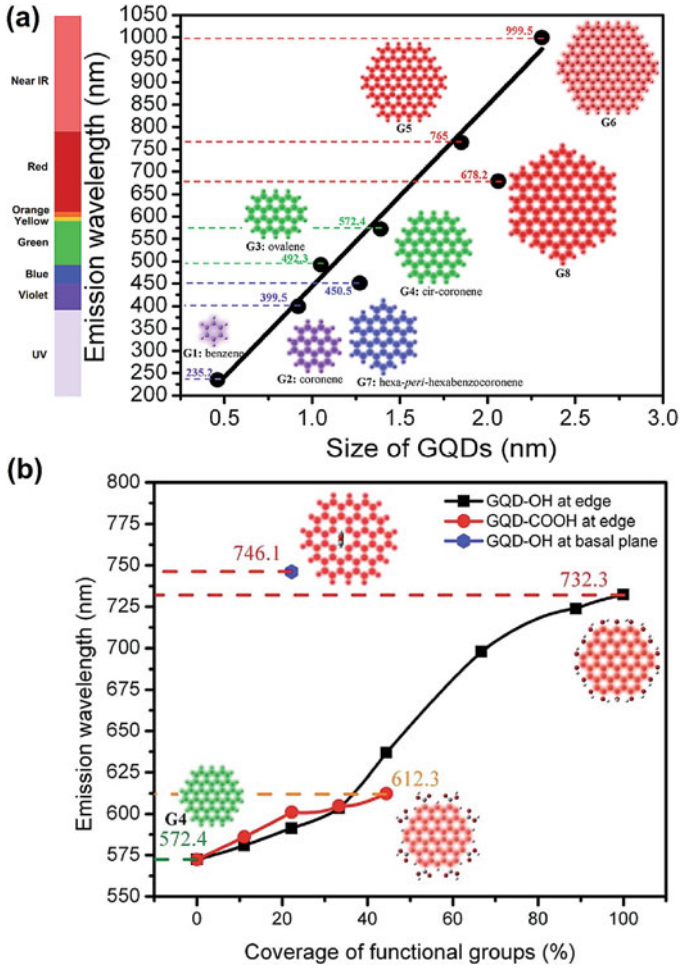

Fig. 7.18 (**a**) Calculated emission wavelength (nm) using TDDFT method in vacuum as a function of the diameter of GQDs. The solid line is the linear fitting of zigzag-edged GQDs (G1–G6). The indicated diameter is the average of the horizontal and vertical dimensions. (**b**) Emission wavelength of oxidized GQD (G4) as a function of the coverage of –OH and –COOH groups. (Reproduced from Ref. [141] with permission of the Royal Society Chemistry)

indicating that the entire visible light emissions (400–770 nm) may be covered by the diameter of GQD while varying from 0.89 to 1.80 nm. The red shift of the emission wavelength, as the size increases, is due to the decrease in band gap resulting from π-electron delocalization [141]. Moreover, such a band gap reduction may also be caused by the fabrication of functional groups (Fig. 7.18b). Graphene with either zigzag or armchair edges may influence the fluorescence of GQDs; for instance, the 1.27 and 2.06 nm armchair-edged GQDs emit at blue-shifted wavelength of ~450.5 and 678.2 nm, respectively, whereas the zigzag-edged GQDs

emit at red-shifted wavelength of ~551 and 872 nm, respectively. The observed results are well related to experimental results reported by Kim et al. supporting the observed blue- and red-shift emission based on the armchair- and zigzag-edged configuration of GQDs [142]. Furthermore, the pyridinic and pyrrolic N-doping on GQDs causes slight blue shift of emission wavelength in a concentration-dependent behavior. Previously, Jin et al. reported the band gap tuning of GQDs through the charge effect of functional groups using DFT analysis with the atomic orbital-based $Dmol^3$ software package [143]. The band gap was predicted to decrease for the functionalization of GQD with one amine group, and further decrease with increase of the number of amine groups (Fig. 7.19a), due to the increased electron density in a GQD-$(NH_2)_n$. As shown in Fig. 7.19b, the energy levels for HOMO state of GQD

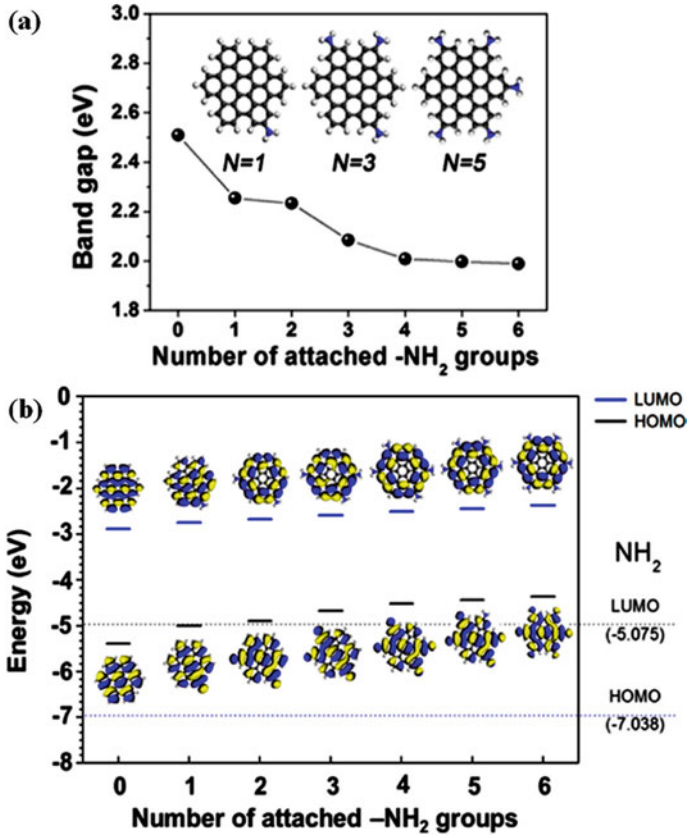

Fig. 7.19 (**a**) Band gap change of GQD-$(NH_2)_n$ as function of the number of attached NH_2 groups (inset images are optimized configuration of GQD-$(NH_2)_n$), (gray, C; white, H and blue, N atom), and (**b**) HOMO and LUMO energy levels of GQDs-$(NH_2)_n$. black and blue lines indicate HOMO and LUMO levels of GQDs-$(NH_2)_n$, respectively. The dotted lines denote the HOMO and LUMO energy level of NH_2. Insets describe HOMO and LUMO isosurface of each system (the isovalue is 0.01 e/Å3). (Reproduced from Ref. [143] with permission of the American Chemical Society)

and the LUMO state of amine group are almost identical, though the energy level of the GQD HOMO state becomes gradually higher than the amine LUMO state as a result of increasing number of NH_2 groups which leads to the difference in the band gap of GQD [143].

Similar to GQDs, the fluorescence of C-dots is originated from the diverse factors such as quantum confinement effect, carbon core effect, surface states, defect/trap sites, and heteroatom/element doping [132–136]. Even so, it was verified that the multi-emission of C-dots was predominated by the carbon core and surface states. The shorter wavelength emissions are mainly due to the recombination of electron-hole pairs in the carbon core, whereas the longer wavelength emissions originate from the surface states [132]. The carbon core in C-dots is mainly composed of sp^2 carbon clusters in the amorphous state. To understand the fluorescing mechanism originated from carbon core, Zhu et al. have analyzed the carbon core structure where the Gaussian 09 package (B3LYP/6-31G(d)) was used to optimize the electronic structures and calculate the energies of frontier molecular orbitals [144]. They used two different model compounds of fused aromatic rings (FARs) and cyclo-1,4-naphthylenes with different C-dots microstructure corresponding to graphitized carbon core (class I) and disordered carbon core (class II), respectively. The energy gaps between the HOMO and LUMO for the class I were calculated to be 2.82 and 1.63 eV for FAR-19 (1.2 nm) and FAR-61 (2.2 nm), respectively. But the inverse trend was calculated for the class II to be 2.80 and 3.46 eV for CN-8 (1.5 nm) and CN-16 (2.7 nm), respectively. From these calculation data regarding the size-dependency of C-dots fluorescence, it can be concluded that for the C-dots with a graphitized core, the smaller the size of the core, the higher the PL energy, while an inverse trend is observed for C-dots with an amorphous core.

Apart from the carbon core, the fluorescence was controlled by the surface states caused by the surface passivation with small organic molecules. The functional groups possess different energy levels leading to the various emissive states on the surface. Upon excitation of functionalized C-dots at certain excitation wavelength, the domination of surface emissive states generally generates fluorescence at the longer wavelength as compared to the fluorescence emitted by carbon core. Dhenadhayalan et al. have studied the effect of surface functional groups (-COOH and $–NH_2$) on the fluorescence of C-dots using time-resolved fluorescence spectroscopy techniques [132]. The surface functional groups are capable of regulating the multi-fluorescence behavior based on the electron-withdrawing and -donating properties of functional groups. The electron transfer takes place from the carbon core to surface domain by the presence of $-$COOH on the surface and vice versa for the case of $-NH_2$ present on the surface. Hola et al. have reported the red-shifted emission for the carboxylic functionalized C-dots [145]. Further, they have analyzed coronene derivatives as a model system to understand the influence of functional groups using TDDFT computation. The maximum emission of functionalized coronene (tricarboxylcoronene, ester of tricarboxylcoronene) was calculated to red shift with respect to that of coronene, as a result of an extension of π-conjugated electrons system. Moreover, upon the addition of carboxyl groups, the electrostatic potential surfaces show a shift of charge toward the edge. This

significant contribution of electrostatic interactions of the surface carboxyl groups greatly influences the role of C-dots acting as surface emissive traps. Similarly, the fluorescence of *para*-substituted anilines functionalized C-dots was controlled to emit at longer wavelength with very narrow spectral width by creating a new energy levels [146].

Different from surface functionalization, the metal/element doping is another important factor to influence the fluorescence properties of C-dots. For instance, Hola et al. have reported graphitic nitrogen triggers red fluorescence in carbon dots accompanied by the results of DFT and TDDFT calculations [147]. The five different pyrene-based models were used for DFT studies which contained carboxyl and hydroxyl groups on the surface and also two graphitic nitrogen inside the pyrene structure as shown in Fig. 7.20. The absorption spectra were computed using the TDDFT with the range-separated hybrid ωB97xD exchange-correlation functional

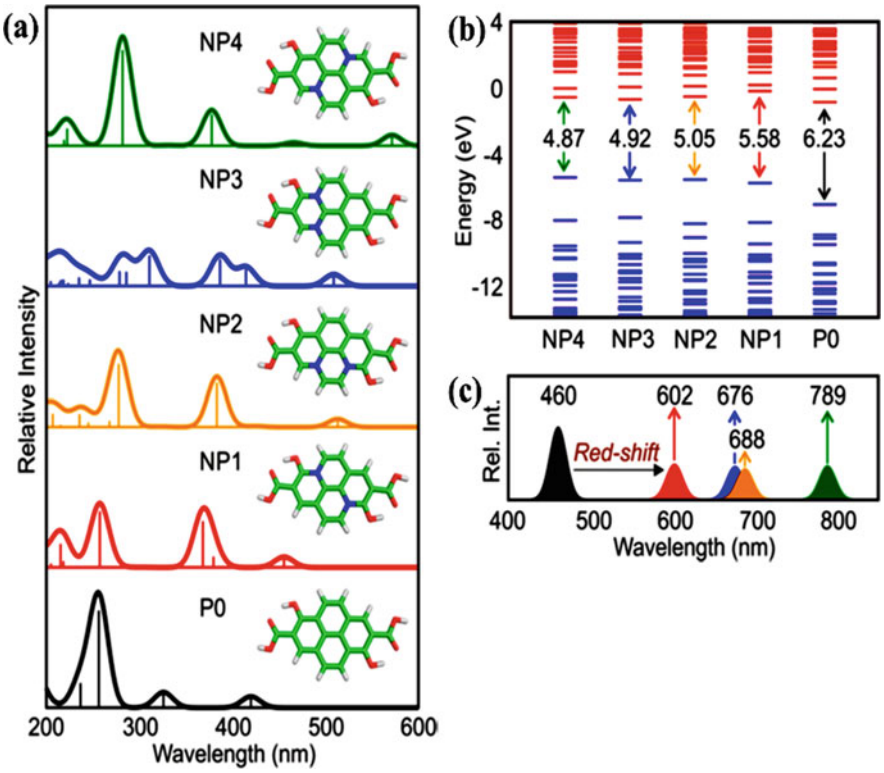

Fig. 7.20 (**a**) Calculated UV-vis absorption spectra for the N-doped models (NP1–NP4) and nitrogen-free system (P0) of the same size: carbon (green), hydrogen (white), oxygen (red), and nitrogen (blue). (**b**) Relative energy levels of the occupied (blue) and unoccupied (red) molecular orbitals of the same structures. (**c**) Model fluorescence spectra of the nitrogen-doped systems NP1 (red), NP2 (orange), NP3 (blue), and NP4 (green) and nitrogen-free system P0 (black). (Reproduced from Ref. [147] with permission of the American Chemical Society)

and 6-31+G(d) basis set. The DFT calculations suggested that the existence of graphitic nitrogen into the carbon core resulted in red-shifted absorption with respect to undoped system which is due to the transition into the second excited singlet state ($S_0 \rightarrow S_2$). Moreover, the differences between the HOMO and LUMO band gap, as shown in Fig. 7.20b, clearly indicate narrowing of the HOMO-LUMO gap in the nitrogen-doped systems and also create mid gap states within the original gap of the undoped system. Consequently, the red-shift fluorescence (above 600 nm) was observed for nitrogen-doped systems (Fig. 7.20c), and the red shift extent gradually increases as increasing amount of graphitic nitrogen in carbon core.

Xu et al. reported the Zn-doped C-dots with a high fluorescence quantum yield (32.3%). The ab initio studies were investigated to understand the involvement of molecular orbitals in the fluorescence process [148]. They have employed two well-established DFT-based ab initio methods including the plane-wave projector-augmented wave method as implemented in the Vienna ab initio simulation package (VASP) and the orthogonalized linear combination of atomic orbital (OLCAO) method. The notable twist in the C-dots structure was observed due to incorporation of Zn on the C-dots surface, as shown in Fig. 7.21a–c, and the Zn dopant may lift up the C-dots surface to move the electronic wave function distribution to the lower side (Fig. 7.21d–e). Moreover, the HOMO and LUMO are loading on the same lower part of C-dots leading to feasible charge transfer from LUMO to HOMO as a result of the binding of Zn with oxygen atoms on the C-dots surface. Then, they have calculated the electronic density of states for Zn-doped C-dots as shown in

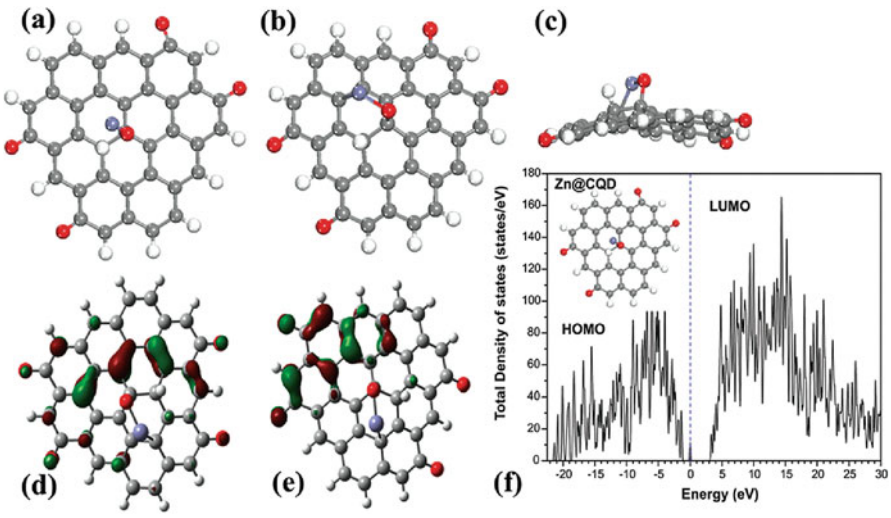

Fig. 7.21 The schematic structure and calculated frontier orbitals for Zn-doped C-dots, with C, H, and O indicated as gray, white, and red spheres. (**a**) Top view of the unrelaxed structure; (**b**) top view of the relaxed structure; (**c**) side view of the relaxed structure; (**d**) HOMO; (**e**) LUMO of Zn-doped C-dots; and (**f**) total density of states of Zn-doped C-dots. (Reproduced from Ref. [148] with permission of the Royal Society Chemistry)

Fig. 7.21f. The Zn-induced state was observed in the middle of the band gap which indicates that the dangling bonds of ionic Zn act as an energy gradient. Due to this intermediate state, the electrons or holes can efficiently move to the surface of C-dots which enhances the charge transfer, thereby resulting in the higher fluorescence quantum yield.

7.5.2 Sensing Analysis of Graphene Quantum Dots and Carbon Dots

The design and fabrication of new fluorescent chemosensors have been developed enormously since successful synthesis of carbon nanomaterials last decade [149–153]. There are two fundamental moieties which merged to obtain the fluorescent chemosensor, composed of the recognition site and the fluorescence signaling source. It is possible to develop a specific fluorescent sensor by switching these two moieties, thereby yielding a strong stable fluorescence signal with high specificity and enhancing the ability for detection of analyte. Generally, the fluorescent sensor materials should have multiple features such as ease for preparation and functionalization, high quantum yield with tunable absorption and fluorescence properties, reliable photostability, non-toxicity, and capability of sensing an analyte at lower detection limit. The GQDs and C-dots exhibit aforementioned unique merits and deserve a wide attention for the application of prospective sensors. To date, the GQDs and C-dots have been extensively utilized as a fluorescence sensing probes to detect analytes including inorganic metal cations and anions, nitro explosives, pesticides, drugs, toxic organic molecules, and important biomolecules based on the fluorescence turn-on and/or turn-off mechanisms. A diverse form of chemical functionalization of these nanomaterials is required in order that their functional properties might be involved in the detection of analytes. Indeed, a variety of analytes could be detected selectively by simply tuning the different functional groups on the surface of nanomaterial. The process of surface functionalization is of crucial importance to impart desired properties to nanomaterials for their applications. The functionalization of nanomaterials can be achieved through either covalent or noncovalent modification techniques. Rich functional groups including carboxylic, amine, alcohol, and thiol groups and also functional small molecules can attach on the surface of nanomaterials to improve their optical properties by controlling the energy gap and electronic properties. Moreover, formation of metal/element doping (N, S, transition metals, etc.) and composites/hybrids (with noble nanoparticles, metal oxides, etc.) with nanomaterials were applied to enhance their inherent properties to expand the application range.

For instance, the S-doped GQDs show the improved electronic properties and surface chemical reactivities compared with that of GQDs, and thereby can be used as an efficient fluorescent probe for highly selective and sensitive detection of Fe^{3+}, reported by Li et al. [153]. The DFT calculations (B3LYP/6-31G*) that the

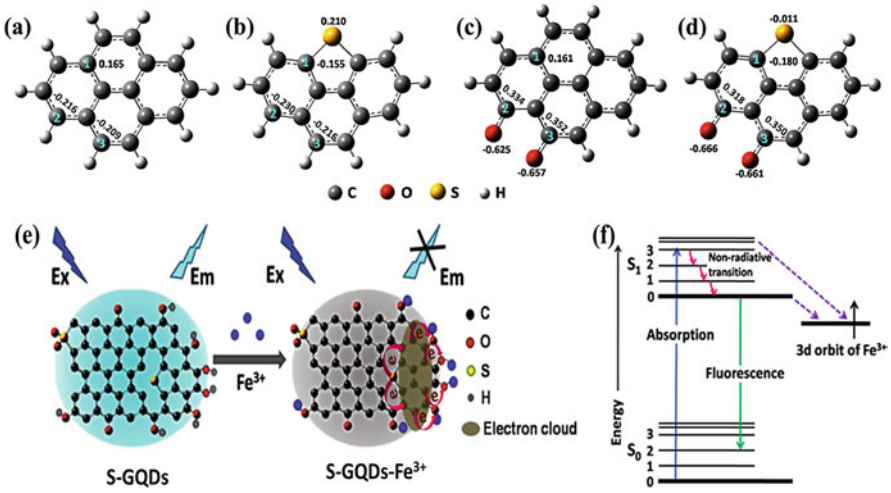

Fig. 7.22 The theoretical models of (**a**, **c**) GQDs and (**b**, **d**) S-GQDs. (**e**) Fluorescence quenching mechanism of the S-GQDs in the presence of Fe^{3+} and (**f**) the electron transfer process from S-GQDs to Fe^{3+}. (Reproduced from Ref. [153] with permission of the American Chemical Society)

electronic density of GQDs was effectively modulated due to doping of S atoms into the conjugated carbon skeleton of GQDs. As shown in Fig. 7.22a–d, four models of GQDs (a, c) and S-GQDs (b, d) were implemented, and the charge density of the representative atoms are shown in black numbers. The S atom directly bonded with C(1) atom enhances the electron density significantly due to the electron-donating ability of S atom, such that the electron densities of C(2) and C(3) atoms increased (Fig. 7.22a, b) as compared with those of undoped GQDs. In contrast, the electron densities of O atoms might increase while bonded to C(2) and C(3) atoms (Fig. 7.22c, d), due to its electron-withdrawing ability thereby enhancing surface electron densities along with S atoms. Therefore, Fe^{3+} ions were efficiently coordinated with phenolic hydroxyl groups on the edge of S-GQDs (Fig. 7.22e) and the electrons transferred from the excited state of S-GQDs to the half-filled 3*d* orbits of Fe^{3+} (Fig. 7.22f), resulting in the fluorescence quenching of S-GQDs.

The detection of chemical explosives has become important issue due to their impact on the environment pollution [154]. The explosives do not have fluorescent properties, and thus the fluorescence-based explosive sensors still dominated over other sensing techniques. The GQDs and C-dots have been used as fluorescence probe to sensing the chemical explosives with high sensitivity and selectivity. According to the experimental results, the sensing mechanism such as photo-induced electron transfer, fluorescence resonance energy transfer, inner filter effect, and intermolecular charge transfer for the fluorogenic detection of explosives was proposed based on the change in the fluorescence properties [154]. Indeed, to understand the accurate sensing mechanism, theoretical studies are needed to integrate the electronic structures. Ju et al. have proved that there were two

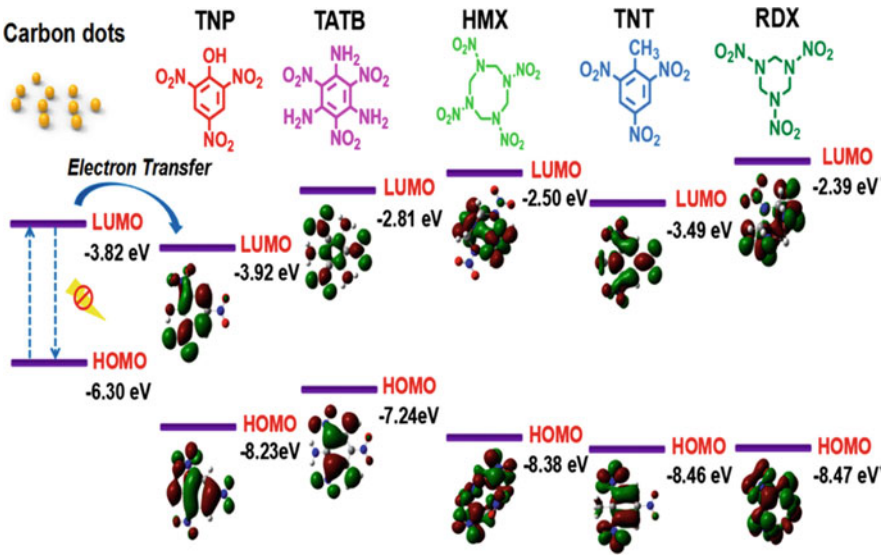

Fig. 7.23 HOMO and LUMO energy levels of C-dots and nitro explosives. (Reproduced from Ref. [155] with permission of the Royal Society Chemistry)

kinds of electron transfer based detection of 2,4,6-trinitrophenol (TNP) using C-dots as fluorescent probe through theoretical calculations along with spectroscopic studies [155]. As shown in Fig. 7.23, the HOMO and LUMO energy levels were calculated for C-dots and various nitro explosives using the B3LYP/6-31G-(d,p) method (Gaussian 09). The obtained results show that the LUMO levels of C-dots ($E_{LUMO} = -3.82$ eV) are higher than that of TNP ($E_{LUMO} = -3.92$ eV) which facilitates the electron transfer from the LUMO of C-dots to the LUMO of TNP resulting in the fluorescence quenching of C-dots. On the other hand, the respective electron transfer is not feasible to other explosives due to a higher LUMO energy level than that of C-dots. Thus, the high sensitivity and selectivity of CDs toward TNP can be ascribed to their efficient ET. Moreover, the theoretical studies confirmed that two kinds of electron transfer processes involve in the detection of TNP such as proton transfer-assisted and hydrogen-bond interaction-assisted electron transfer.

7.6 Conclusions

Since the rapid development in the number of studies related to the applications of functionalized graphene-based metal-free heterogeneous catalysis, rather than attempting to summarize all the progress achieved to date, we discuss the role of metal-free graphene and its derivatives with particular emphasis on the influence of

defects and functional groups on their interaction with catalytic phases, as well as the advantages of structures in the electron/mass transfer process. Additionally, we provide a comprehensive summary on the contribution of edges/defects, functional groups, and doping structures to the intrinsic catalytic properties of graphene-based metal-free catalysts.

Recently, the fluorescence mechanism of GQDs and C-dots has been extensively resolved by experiments with some theoretical calculations. The fluorescence properties of GQDs and C-dots turn out to be sensitive to their size, defects, edge configuration, surface functional groups, heteroatom/element dopant, etc. The DFT calculations are significantly helpful with the understanding about the fluorescence properties of GQDs and C-dots. However, restricted to complicated involvement of several factors, there is a room left for further investigation to gain better theoretical understanding of fluorescence properties which could assist to design and develop new advanced functional nanomaterials as well as enhance their applications.

7.7 Outlook

This book chapter highlights the important developments of functional carbon nanomaterials for these most distinguished organic transformations by using DFT methods. Notably, DFT is widely used in structure prediction, defects, phase stability, property prediction, and screening for many industrially and biologically important reactions. Thanks to the effective efforts of scientists and researchers in DFT-related fields, much progress has been achieved in the direction of the synthesis and characterization of these functional carbon nanomaterials and their applications to various organic transformations. Among these materials, the porous carbon materials have been the main choice for carbon nanomaterials in catalytic applications, because of their special physiochemical properties, including large surface area and pore volumes, active sites, low toxicity, and chemically modifiable surfaces. The application of DFT in functional carbon nanomaterial-related chemistry helps design catalytically across a range of homogeneous and heterogeneous catalysts. A variety of surface functional groups can be generated upon the bonding or doping of heteroatoms such as N, O, P, S, B, etc., to defects in metal-free carbon catalysts. Although focusing on electrostatic environmental effects may open new routes toward the rational optimization of efficient catalysts, much more predictive capacity is required with theoretical methods to have a transformative impact in their computational design as well as fulfill the concept of sustainable chemistry which should be the main objectives for future research and development (R&D). Moreover, in that context significant stimulation and progress may also be expected from virtual exploration and massive in DFT for the field of functional carbon nanomaterials in near future.

Apart from the utilization of carbon nanomaterials in the fields of catalysis and chemosensors, nowadays the usage of nanomaterials in biosensor has gained a great importance and explored for point-of-care applications. The unique inherent prop-

erties of carbon nanomaterials especially 0D of C-dots and GQDs, 1D of CNTs, and 2D of graphene have extensively employed toward the development of biosensors. When applying carbon nanomaterials with biomolecules, a significant improvement can be achieved in characteristics of biosensors such as high selectivity and sensitivity, biocompatibility, non-toxicity, and fast response. The biomolecules including proteins, DNA, antibody, and enzyme can be easily associated with functionalized carbon nanomaterials through covalent and/or electrostatic interactions. Due to the strong specificity of carbon nanomaterials with biomolecules, they provide an excellent advantage for biosensors by detecting a specific target biomolecules with higher sensitivity. The other important characteristics of carbon nanomaterials are low toxicity, good biocompatibility, as well as superior resistance to photobleaching which make them good candidates for the development of biosensors.

From the viewpoint of fluorescence experiments, the interaction between the carbon nanomaterials (GQDs and C-dots) and biomolecules occurs via due to the hydrophobic and/or electrostatic interaction, and the corresponding sensing mechanism proposed is based on the fluorescence change. However, understanding the precise role of carbon nanomaterials in interacting with the biomolecules still need to be discovered. Thus there is a good reason for further development of fluorescence carbon nanomaterial-based biosensors. As such a future trend is to better understand the relation between the probe and analyte, and the sensing mechanism. In addition to experiments, the theoretical simulation studies will play a major role in future to potentially solve the issues related to fundamental understanding about the fluorescence of carbon nanomaterials, sensing mechanism, etc. To achieve this goal, the integrating theoretically the complete structure of GQDs and C-dots is necessary in accordance with the core moiety, size, shape, and functional groups, so that it can help to predict the accurate interaction between the sensing materials and biomolecules from a theoretical perspective. The sensing performance would be significantly improved by regulating the properties of sensing materials including size, shape, functional groups, electronic structures, optical absorption and emission, and redox properties. The information from the theoretical aspects can be aid to design the new and unique materials to sensing the specific biomolecules with higher selectivity and sensitivity. We believe that theoretical simulation and modelling studies of fluorescence-based biosensors will have a promising future.

References

1. L.A. Curtiss, P.C. Redfern, K. Raghavachari, Assessment of Gaussian-3 and density-functional theories on the G3/05 test set of experimental energies. J. Chem. Phys. **123**, 124107 (2005)
2. R.K. Raju, A. Ramraj, I.H. Hillier, M.A. Vincent, N.A. Burton, Carbohydrate-aromatic pi interactions: A test of density functionals and the DFT-D method. Phys. Chem. Chem. Phys. **11**, 3411–3416 (2009)

3. P. Liu, Y. Zhao, R. Qin, S. Mo, G. Chen, L. Gu, D.M. Chevrier, P. Zhang, Q. Guo, D. Zang, B. Wu, G. Fu, N. Zheng, Photochemical route for synthesizing atomically dispersed palladium catalysts. Science **352**, 797–801 (2016)
4. J.K. Nørskov, M. Scheffler, H. Toulhoat, Density functional theory in surface science and heterogeneous catalysis. MRS Bull. **31**, 669–674 (2006)
5. J.K. Norskov, T. Bligaard, J. Rossmeisl, C.H. Christensen, Towards the computational design of solid catalysts. Nat. Chem. **1**, 37–46 (2009)
6. B.D. Dunnington, J.R. Schmidt, A projection-free method for representing plane-wave DFT results in an atom-centered basis. J. Chem. Phys. **143**, 104109 (2015)
7. E.J. Bylaska, M. Valiev, R. Kawai, J.H. Weare, Parallel implementation of the projector augmented plane wave method for charged systems. Comput. Phys. Commun. **143**, 11–28 (2002)
8. E.J. Bylaska, Plane-wave DFT methods for chemistry. Annu. Rep. Comput. Chem. **13**, 185–228 (2017)
9. R. Das, N. Dhar, A. Bandyopadhyay, D. Jana, Size dependent magnetic and optical properties in diamond shaped graphene quantum dots: A DFT study. J. Phys. Chem. Solids **99**, 34–42 (2016)
10. V. Cantatore, I. Panas, Communication: Towards catalytic nitric oxide reduction via oligomerization on boron doped graphene. J. Chem. Phys. **144**, 151102 (2016)
11. H.R. Jiang, T.S. Zhao, L. Shi, P. Tan, L. An, First-principles study of nitrogen-, boron-doped graphene and co-doped graphene as the potential catalysts in nonaqueous Li-O_2 batteries. J. Phys. Chem. C **120**, 6612–6618 (2016)
12. L. Ferrighi, M. Datteo, C. Di Valentin, Boosting graphene reactivity with oxygen by boron doping: Density functional theory modeling of the reaction path. J. Phys. Chem. C **118**, 223–230 (2014)
13. R.G. Parr, W. Yang, *Density-Functional Theory of Atoms and Molecules* (Oxford University Press, Oxford, 1989)
14. W. Koch, M.C. Holthausen, *A Chemist's Guide to Density Functional Theory* (Wiley-VCH, New York, 2001)
15. Q. Liu, Z.S. Li, S.L. Chen, Metal-embedded graphene as potential counter electrode for dye-sensitized solar cell. Ind. Eng. Chem. Res. **55**, 455–462 (2016)
16. X. Chen, F. Li, N. Zhang, L. An, D. Xia, Mechanism of oxygen reduction reaction catalyzed by Fe(Co)-Nx/C. Phys. Chem. Chem. Phys. **15**, 19330–19336 (2013)
17. W.B. Schneider, U. Benedikt, A.A. Auer, Interaction of platinum nanoparticles with graphitic carbon structures: A computational study. ChemPhysChem **14**, 2984–2989 (2013)
18. J. Kang, J.S. Yu, B. Han, First-principles design of graphene based active catalysts for oxygen reduction and evolution reactions in the aprotic Li-O_2 battery. J. Phys. Chem. Lett. **7**, 2803–2808 (2016)
19. S. Navalon, A. Dhakshinamoorthy, M. Alvaro, M. Antonietti, H. García, Active sites on graphene-based materials as metal-free catalysts. Chem. Soc. Rev. **46**, 4501–4529 (2017)
20. X. Duan, Z. Ao, L. Zhou, H. Sun, G. Wang, S. Wang, Occurrence of radical and nonradical pathways from carbocatalysts for aqueous and nonaqueous catalytic oxidation. Appl. Catal. B **188**, 98–105 (2016)
21. J. Vazquez-Arenas, G. Ramos-Sanchez, A.A. Franco, A multiscale model of the oxygen reduction reaction on highly active graphene nanosheets in alkaline conditions. J. Power Sources **328**, 492–502 (2016)
22. S. Mussell, P. Choudhury, Density functional theory study of iron phthalocyanine porous layer deposited on graphene substrate: A Pt-free electrocatalyst for hydrogen fuel cells. J. Phys. Chem. C **120**, 5384–5391 (2016)
23. X. Guo, G. Fang, G. Li, H. Ma, H. Fan, L. Yu, C. Ma, X. Wu, D. Deng, M. Wei, D. Tan, R. Si, S. Zhang, J. Li, L. Sun, Z. Tang, X. Pan, X. Bao, Direct, nonoxidative conversion of methane to ethylene, aromatics, and hydrogen. Science **344**, 616–619 (2014)

24. R.S. Assary, P.C. Redfern, J.R. Hammond, J. Greeley, L.A. Curtiss, Computational studies of the thermochemistry for conversion of glucose to levulinic acid. J. Phys. Chem. B **114**, 9002–9009 (2010)
25. L.A. Curtiss, P.C. Redfern, K. Raghavachari, Gaussian-4 theory using reduced order perturbation theory. J. Chem. Phys. **127**, 124105 (2007)
26. G.I. Csonka, A.D. French, G.P. Johnson, C.A. Stortz, Evaluation of density functionals and basis sets for carbohydrates. J. Chem. Theory Comput. **5**, 679–692 (2009)
27. S. Bertelsen, K.A. Jørgensen, Organocatalysis-after the gold rush. Chem. Soc. Rev. **38**, 2178–2189 (2009)
28. O. Mohammadi, M. Golestanzadeh, M. Abdouss, Recent advances in organic reactions catalyzed by graphene oxide and sulfonated graphene as heterogeneous nanocatalysts: A review. New J. Chem. **41**, 11471–11497 (2017)
29. D.V. Boukhvalov, D.R. Dreyer, C.W. Bielawski, Y.-W. Soon, A computational investigation of the catalytic properties of graphene oxide: Exploring mechanisms by using DFT methods. ChemCatChem **4**, 1844–1849 (2012)
30. V.S. Jeyaraj, M. Kamaraj, V. Subramanian, Generalized reaction mechanism for the selective aerobic oxidation of aryl and alkyl alcohols over nitrogen-doped graphene. J. Phys. Chem. C **119**, 26438–26450 (2015)
31. B. Dai, K. Chen, Y. Wang, L. Kang, M. Zhu, Boron and nitrogen doping in graphene for the catalysis of acetylene hydrochlorination. ACS Catal. **5**, 2541–2547 (2015)
32. H. Yang, X. Cui, X. Dai, Y. Deng, F. Shi, Carbon-catalysed reductive hydrogen atom transfer reactions. Nat. Commun. **6**, 6478 (2015)
33. D.R. Dreyer, C.W. Bielawski, Carbocatalysis: Heterogeneous carbons finding utility in synthetic chemistry. Chem. Sci. **2**, 1233–1240 (2011)
34. X. Wu, Z. Xie, M. Sun, T. Lei, Z. Zuo, X. Xie, Y. Liang, Q. Huang, Edge-rich and (N, S)-doped 3D porous graphene as an efficient metal-free electrocatalyst for the oxygen reduction reaction. RSC Adv. **6**, 90384–90387 (2016)
35. Y. Zhao, S. Huang, M. Xia, S. Rehman, S. Mu, Z. Kou, Z. Zhang, Z. Chen, F. Gao, Y. Hou, N-P-O co-doped high performance 3D graphene prepared through red phosphorous-assisted "cutting-thin" technique: A universal synthesis and multifunctional applications. Nano Energy **28**, 346–355 (2016)
36. H. Wang, K. Sun, F. Tao, D.J. Stacchiola, Y.H. Hu, 3D honeycomb-like structured graphene and its high efficiency as a counter-electrode catalyst for dye-sensitized solar cells. Angew. Chem. Int. Ed. **52**, 9210–9214 (2013)
37. D. Deng, L. Yu, X. Pan, X. Wang, X. Chen, P. Hu, L. Sun, X. Bao, Size effect of graphene on electrocatalytic activation of oxygen. Chem. Commun. **47**, 10016–10018 (2011)
38. D. Deng, K.S. Novoselov, Q. Fu, N. Zheng, Z. Tian, X. Bao, Catalysis with two-dimensional materials and their heterostructures. Nat. Nanotechnol. **11**, 218–230 (2016)
39. F. Yang, D. Deng, X. Pan, Q. Fu, X. Bao, Understanding nano effects in catalysis. Natl. Sci. Rev. **2**, 183–201 (2015)
40. W. Koch, M.C. Holthausen, *A Chemist's Guide to Density Functional Theory* (Wiley VCH, Weinheim, 2001)
41. W. Kohn, Nobel lecture: Electronic structure of matter–wave functions and density functionals. Rev. Mod. Phys. **71**, 1253 (1998)
42. R.O. Jones, O. Gunnarsson, The density functional formalism, its applications and prospects. Rev. Mod. Phys. **61**, 689 (1989)
43. P. Veerakumar, P. Thanasekaran, K.-L. Lu, K.-C. Lin, S. Rajagopal, Computational studies of versatile heterogeneous palladium catalyzed Suzuki, Heck, and Sonogashira coupling reactions. ACS Sustain. Chem. Eng. **5**, 8475–8490 (2017)
44. V.V. Welborn, L.R. Pestana, T. Head-Gordon, Computational optimization of electric fields for better catalysis design. Nat. Catal. **1**, 649–655 (2018)
45. B. Liu, H. Li, X. Ma, R. Chen, S. Wang, L. Li, The synergistic effect of oxygen-containing functional groups on CO_2 adsorption by the glucose–potassium citrate-derived activated carbon. RSC Adv. **8**, 38965–38973 (2018)

46. G. Lim, K.B. Lee, H.C. Ham, Effect of N-containing functional groups on CO_2 adsorption of carbonaceous materials: A density functional theory approach. J. Phys. Chem. C **120**, 8087–8095 (2016)
47. S. Grimme, Semiempirical GGA-type density functional constructed with a long-range dispersion correction. J. Comput. Chem. **27**, 1787–1799 (2006)
48. X. Wang, Y. Liu, X. Ma, S.K. Das, M. Ostwal, I. Gadwal, K. Yao, X. Dong, Y. Han, I. Pinnau, Soluble polymers with intrinsic porosity for flue gas purification and natural gas upgrading. Adv. Mater. **29**, 1605826 (2017)
49. P. Geerlings, F. De Proft, W. Langenaeker, Conceptual density functional theory. Chem. Rev. **103**, 1793–1874 (2003)
50. A. Zangwill, The education of Walter Kohn and the creation of density functional theory. Arch. Hist. Exact Sci. **68**, 775–848 (2014)
51. R.O. Jones, Density functional theory: Its origins, rise to prominence, and future. Rev. Mod. Phys. **87**, 897–923 (2015)
52. E. Furimsky, Graphene-derived supports for hydroprocessing catalysts. Ind. Eng. Chem. Res. **56**, 11359–11371 (2017)
53. B.C. Thompson, E. Murray, G.G. Wallace, Graphite oxide to graphene. Biomaterials to bionics. Adv. Mater. **27**, 7563–7582 (2015)
54. Z. Huang, H. Zhou, W. Yang, C. Fu, L. Chen, Y. Kuang, Three-dimensional hierarchical porous nitrogen and sulfur-codoped graphene nanosheets for oxygen reduction in both alkaline and acidic media. ChemCatChem **9**, 987–996 (2017)
55. I. Shimoyama, Y. Baba, Thiophene adsorption on phosphorus and nitrogen-doped graphites: Control of desulfurization properties of carbon materials by heteroatom doping. Carbon **98**, 115–125 (2016)
56. M. Gomez-Martínez, A. Baeza, D.A. Alonso, Pinacol rearrangement and direct nucleophilic substitution of allylic alcohols promoted by graphene oxide and graphene oxide CO_2H. ChemCatChem **9**, 1032–1039 (2017)
57. H. Ahmad, M. Fan, D. Hui, Graphene oxide incorporated functional materials: A review. Compos. Part B **145**, 270–280 (2018)
58. S. Ren, P. Rong, Q. Yu, Preparations, properties and applications of graphene in functional devices: A concise review. Ceram. Int. **44**, 11940–11955 (2018)
59. M. Sun, J. Li, Graphene oxide membranes: Functional structures, preparation and environmental applications. Nano Today **20**, 121–137 (2018)
60. L. Zhang, Q. Xu, J. Niu, Z. Xia, Role of lattice defects in catalytic activities of graphene clusters for fuel cells. Phys. Chem. Chem. Phys. **17**, 16733–16743 (2015)
61. Z. Zhao, M. Li, L. Zhang, L. Dai, Z. Xia, Design principles for heteroatom-doped carbon nanomaterials as highly efficient catalysts for fuel cells and metal–air batteries. Adv. Mater. **27**, 6834–6840 (2015)
62. Y. Zheng, Y. Jiao, Y. Zhu, L.H. Li, Y. Han, Y. Chen, A. Du, M. Jaroniec, S.Z. Qiao, Hydrogen evolution by a metal-free electrocatalyst. Nat. Commun. **5**, 3783 (2014)
63. C.J. Paez, A.L.C. Pereira, J.N.B. Rodrigues, N.M.R. Peres, Electronic transport across linear defects in graphene. Phys. Rev. B–Condens. Matter Mater. Phys. **92**, 045426 (2015)
64. L. Zhang, Z. Xia, Mechanisms of oxygen reduction reaction on nitrogen-doped graphene for fuel cells. J. Phys. Chem. C **115**, 11170–11176 (2011)
65. G.L. Tian, M.Q. Zhao, D. Yu, X.Y. Kong, J.Q. Huang, Q. Zhang, F. Wei, Nitrogen-doped graphene/carbon nanotube hybrids: In situ formation on bifunctional catalysts and their superior electrocatalytic activity for oxygen evolution/reduction reaction. Small **10**, 2251–2259 (2014)
66. C.L. Su, K.P. Loh, Carbocatalysts: Graphene oxide and its derivatives. Acc. Chem. Res. **46**, 2275–2285 (2013)
67. L. Lai, J.R. Potts, D. Zhan, L. Wang, C.K. Poh, C. Tang, H. Gong, Z. Shen, J. Lin, R.S. Ruoff, Exploration of the active center structure of nitrogen-doped graphene-based catalysts for oxygen reduction reaction. Energy Environ. Sci. **5**, 7936–7942 (2012)

68. B.F. Machado, P. Serp, Graphene-based materials for catalysis. Catal. Sci. Technol. **2**, 54–75 (2012)
69. D.R. Dreyer, H.P. Jia, C.W. Bielawski, Graphene oxide: A convenient carbocatalyst for facilitating oxidation and hydration reactions. Angew. Chem. Int. Ed. **49**, 6813–6816 (2010)
70. H.P. Jia, D.R. Dreyer, C.W. Bielawski, C-H oxidation using graphite oxide. Tetrahedron **67**, 4431–4434 (2011)
71. X.Y. Sun, P. Han, B. Li, S.J. Mao, T.F. Liu, S. Ali, Z. Lian, D.S. Su, Oxidative dehydrogenation reaction of short alkanes on nanostructured carbon catalysts: A computational account. Chem. Commun. **54**, 864–875 (2018)
72. X. Liu, B. Frank, W. Zhang, T.P. Cotter, R. Schlögl, D.S. Su, Carbon-catalyzed oxidative dehydrogenation of n-butane: Selective site formation during sp^3-to-sp^2 lattice rearrangement. Angew. Chem. Int. Ed. **50**, 3318–3332 (2011)
73. L. Roldan, A.M. Benito, E. Garcıa-Bordeje, Self-assembled graphene aerogel and nanodiamond hybrids as high performance catalysts in oxidative propane dehydrogenation. J. Mater. Chem. A **3**, 24379–24388 (2015)
74. B. Frank, R. Blume, A. Rinaldi, A. Trunschke, R. Schlögl, Oxygen insertion catalysis by sp^2 carbon. Angew. Chem. Int. Ed. **50**, 10226–10230 (2011)
75. O.V. Khavryuchenko, B. Frank, A. Trunschke, K. Hermann, R. Schlögl, Quantum-chemical investigation of hydrocarbon oxidative dehydrogenation over spin-active carbon catalyst clusters. J. Phys. Chem. C **117**, 6225–6234 (2013)
76. S. Ni, Z. Li, J. Yang, Oxygen molecule dissociation on carbon nanostructures with different types of nitrogen doping. Nanoscale **4**, 1184–1189 (2012)
77. S.B. Tang, Z.X. Cao, Site-dependent catalytic activity of graphene oxides towards oxidative dehydrogenation of propane. Phys. Chem. Chem. Phys. **14**, 16558–16565 (2012)
78. L. Favaretto, J. An, M. Sambo, A.D. Nisi, C. Bettini, M. Melucci, A. Kovtun, A. Liscio, V. Palermo, A. Bottoni, F. Zerbetto, M. Calvaresi, M. Bandini, Graphene oxide promotes site-selective allylic alkylation of thiophenes with alcohols. Org. Lett. **20**, 3705–3709 (2018)
79. C. Su, M. Acik, K. Takai, J. Lu, S.-J. Hao, Y. Zheng, P. Wu, Q. Bao, T. Enoki, Y.J. Chabal, K.P. Loh, Probing the catalytic activity of porous graphene oxide and the origin of this behaviour. Nat. Commun. **3**, 1298 (2012)
80. Q. Gu, G. Wen, Y. Ding, K.-H. Wu, C. Chen, D. Su, Reduced graphene oxide: A metal-free catalyst for aerobic oxidative desulfurization. Green Chem. **19**, 1175–1181 (2017)
81. R.H. Crabtree, A. Lei, Introduction: CH activation. Chem. Rev. **117**, 8481–8482 (2017)
82. Y. Gao, G. Hu, J. Zhong, Z. Shi, Y. Zhu, D.S. Su, J. Wang, X. Bao, D. Ma, Nitrogen-doped sp^2-hybridized carbon as a superior catalyst for selective oxidation. Angew. Chem. Int. Ed. **52**, 2109–2113 (2013)
83. Y. Gao, P. Tang, H. Zhou, W. Zhang, H. Yang, N. Yan, G. Hu, D. Mei, J. Wang, D. Ma, Graphene oxide catalyzed C-H bond activation: The importance of oxygen functional groups for biaryl construction. Angew. Chem. Int. Ed. **55**, 3124–3128 (2016)
84. J.H. Yang, Y.J. Gao, W. Zhang, P. Tang, J. Tan, A.H. Lu, D. Ma, Cobalt phthalocyanine–graphene oxide nanocomposite: Complicated mutual electronic interaction. J. Phys. Chem. C **117**, 3785–3788 (2013)
85. P. Veerakumar, P. Thanasekaran, K.-C. Lin, S.-B. Liu, Well-dispersed rhenium nanoparticles on three-dimensional carbon nanostructures: Efficient catalysts for the reduction of aromatic nitro compounds. J. Colloid Interface Sci. **506**, 271–282 (2017)
86. X.X. Chen, B.L. Chen, Macroscopic and spectroscopic investigations of the adsorption of nitroaromatic compounds on graphene oxide, reduced graphene oxide, and graphene nanosheets. Environ. Sci. Technol. **49**, 6181–6189 (2015)
87. Y.J. Gao, D. Ma, C.L. Wang, J. Guan, X.H. Bao, Reduced graphene oxide as a catalyst for hydrogenation of nitrobenzene at room temperature. Chem. Commun. **47**, 2432–2434 (2011)
88. T. Lv, S.B. Wu, H. Hong, L. Chen, R.J. Dong, Dynamics of nitrobenzene degradation and interactions with nitrogen transformations in laboratory-scale constructed wetlands. Bioresour. Technol. **133**, 529–536 (2013)

89. N. Pradhan, A. Pal, T. Pal, Silver nanoparticle catalyzed reduction of aromatic nitro compounds. Colloids Surf. A Physicochem. Eng. Asp. **196**, 247–257 (2002)
90. X. Kong, Z. Sun, M. Chen, C. Chen, Q. Chen, Metal-free catalytic reduction of 4-nitrophenol to 4-aminophenol by N doped graphene. Energy Environ. Sci. **6**, 3260–3266 (2013)
91. L. Li, Q. Liu, Y.-X. Wang, H.-Q. Zhao, C.-S. He, H.-Y. Yang, L. Gong, Y. Mu, H.-Q. Yu, Facilitated biological reduction of nitroaromatic compounds by reduced graphene oxide and the role of its surface characteristics. Sci. Rep. **6**, 30082 (2016)
92. Z.M. Summers, H.E. Fogarty, C. Leang, A.E. Franks, N.S. Malvankar, D.R. Lovley, Direct exchange of electrons within aggregates of an evolved syntrophic coculture of anaerobic bacteria. Science **330**, 1413–1415 (2010)
93. F. Liu, A.-E. Rotaru, P.M. Shrestha, N.S. Malvankar, K.P. Nevin, D.R. Lovleya, Promoting direct interspecies electron transfer with activated carbon. Energy Environ. Sci. **5**, 8982–8989 (2012)
94. L. Borchardt, Q.-L. Zhu, M.E. Casco, R. Berger, X. Zhuang, S. Kaskel, X. Feng, Q. Xu, Toward a molecular design of porous carbon materials. Mater. Today **20**, 592–610 (2017)
95. J.L. Figueiredo, Functionalization of porous carbons for catalytic applications. J. Mater. Chem. A **1**, 9351–9364 (2013)
96. D.S. Su, J. Zhang, B. Frank, A. Thomas, X. Wang, J. Paraknowitsch, R. Schlçgl, Metal-free heterogeneous catalysis for sustainable chemistry. ChemSusChem **3**, 169–180 (2010)
97. M.R. Benzigar, S.N. Talapaneni, S. Joseph, K. Ramadass, G. Singh, J. Scaranto, U. Ravon, K. Al-Bahily, A. Vinu, Recent advances in functionalized micro and mesoporous carbon materials: Synthesis and applications. Chem. Soc. Rev. **47**, 2680–2721 (2018)
98. S. Xiaoyan, W. Rui, S. Dangsheng, Research progress in metal-free carbon-based catalysts. Chin. J. Catal. **34**, 508–523 (2013)
99. J. Wang, H. Liu, X. Gu, H. Wang, D.S. Su, Synthesis of nitrogen-containing ordered mesoporous carbon as a metal-free catalyst for selective oxidation of ethylbenzene. Chem. Commun. **50**, 9182–9184 (2014)
100. I. Matos, M. Bernardo, I. Fonseca, Porous carbon: A versatile material for catalysis. Catal. Today **285**, 194–203 (2017)
101. S.S. Barton, M.J.B. Evans, E. Halliop, J.A.F. Macdonald, Acidic and basic sites on the surface of porous carbon. Carbon **35**, 1361–1366 (1997)
102. A. Stergiou, N. Karousis, D.T. Dimitratos, Metal-Free Functionalized Carbons in Catalysis Synthesis, Characterization and Applications, in *Non-covalent Methodologies for the Preparation of Metal-Free Nanocarbons for Catalysis*, (The Royal Society of Chemistry, Cambridge, 2018), pp. 29–66;. ISBN 978-1-78262-863-7
103. P. Serp, B. Machado, *Nanostructured Carbon Materials for Catalysis* (The Royal Society of Chemistry, Cambridge,. ISSN 1757–6725, 2015)
104. M. Naderi, Chapter 14: Surface Area: Brunauer–Emmett–Teller (BET), in *Progress in Filtration and Separation*, ed. by S. Tarleton, (Academic, London, 2015), pp. 585–608
105. P. Tang, G. Hu, M. Li, D. Ma, Graphene-based metal-free catalysts for catalytic reactions in the liquid phase. ACS Catal. **6**, 6948–6958 (2016)
106. X. Li, J. Zhang, W. Li, MOF-derived nitrogen-doped porous carbon as metal-free catalysts for acetylene hydrochlorination. J. Ind. Eng. Chem. **44**, 146–154 (2016)
107. J.L. Figueiredo, M.F.R. Pereira, The role of surface chemistry in catalysis with carbons. Catal. Today **150**, 2–7 (2010)
108. A. Rey, M. Faraldos, A. Bahamonde, J.A. Casas, J.A. Zazo, J.J. Rodrıguez, Role of the activated carbon surface on catalytic wet peroxide oxidation. Ind. Eng. Chem. Res. **47**, 8166–8174 (2008)
109. G. Wen, S. Wu, B. Li, C. Dai, D.S. Su, Active sites and mechanisms for direct oxidation of benzene to phenol over carbon catalysts. Angew. Chem. Int. Ed. **54**, 4105–4109 (2015)
110. Q. Wei, H. Fan, F. Qin, Q. Ma, W. Shen, Metal-free honeycomb-like porous carbon as catalyst for direct oxidation of benzene to phenol. Carbon **133**, 6–13 (2018)

111. L.F. Wang, J. Zhang, D.S. Su, Y.Y. Ji, X.J. Cao, F.S. Xiao, Simple preparation of honeycomb-like macrostructured and microporous carbons with high performance in oxidative dehydrogenation of ethylbenzene. Chem. Mater. **19**, 2894–2897 (2007)
112. L. Pereira, R. Pereira, M.F.R. Pereira, M.M. Alves, Effect of different carbon materials as electron shuttles in the anaerobic biotransformation of nitroanilines. Biotechnol. Bioeng. **113**, 1194–1202 (2016)
113. D.S. Su, S. Perathoner, G. Centi, Nanocarbons for the development of advanced catalysts. Chem. Rev. **113**, 5782–5816 (2013)
114. R.W. Pekala, Organic aerogels from the polycondensation of resorcinol with formaldehyde. J. Mater. Sci. **24**, 3221–3227 (1989)
115. R.P. Rocha, M.F.R. Pereira, J.L. Figueiredo, Carbon as a catalyst: Esterification of acetic acid with ethanol. Catal. Today **218–219**, 51–56 (2013)
116. J.P.S. Sousa, M.F.R. Pereira, J.L. Figueiredo, NO oxidation over nitrogen doped carbon xerogels. Appl. Catal. B **125**, 398–408 (2012)
117. R.P. Rocha, J. Restivo, J.P.S. Sousa, J.J.M. Órfão, M.F.R. Pereira, J.L. Figueiredo, Nitrogen-doped carbon xerogels as catalysts for advanced oxidation processes. Catal. Today **241**, 73–79 (2015)
118. B. Xing, J.J. Pignatello, Sorption of Organic Chemicals, in *Encyclopedia of Soils in the Environment*, ed. by D. Hillel, (Elsevier, Oxford, 2005), pp. 537–548
119. T.W. Kirchstetter, T. Novakov, Controlled generation of black carbon particles from a diffusion flame and applications in evaluating black carbon measurement methods. Atmos. Environ. **41**, 1874–1888 (2007)
120. X.D. Yu, W.W. Gong, X.H. Liu, H.Y. Bao, The reductive mechanism of nitrobenzene catalyzed by nine charcoals in sulfides solution. Sci. China Chem. **55**, 1–7 (2012)
121. H. Amezquita-Garcia, E. Razo-Flores, F. Cervantes, J. Rangel-Mendez, Activated carbon fibers as redox mediators for the increased reduction of nitroaromatics. Carbon **55**, 276–284 (2013)
122. R.P. Schwarzenbach, P.M. Gschwend, D.M. Imboden, *Environmental Organic Chemistry* (Wiley, Hoboken, 2005)
123. W. Gong, X. Liu, S. Xia, B. Liang, W. Zhang, Abiotic reduction of trifluralin and pendimethalin by sulfides in black-carbon-amended coastal sediments. J. Hazard. Mater. **310**, 125–134 (2016)
124. S.Y. Oh, P.C. Chiu, Graphite-and soot-mediated reduction of 2,4-dinitrotoluene and hexahydro-1,3,5-trinitro-1,3,5-triazine. Environ. Sci. Technol. **43**, 6983–6988 (2009)
125. X. Yu, H. Cheng, M. Zhang, Y. Zhao, L. Qu, G. Shi, Graphene-based smart materials. Nat. Rev. Mater. **2**, 17046 (2017)
126. A.J. Clancy, M.K. Bayazit, S.A. Hodge, N.T. Skipper, C.A. Howard, M.S.P. Shaffer, Charged carbon nanomaterials: Redox chemistries of fullerenes, carbon nanotubes, and graphenes. Chem. Rev. **118**, 7363–7408 (2018)
127. A. Narita, X.-Y. Wang, X. Feng, K. Mullen, New advances in nanographene chemistry. Chem. Soc. Rev. **44**, 6616–6643 (2015)
128. V. Georgakilas, J.N. Tiwari, K.C. Kemp, J.A. Perman, A.B. Bourlinos, K.S. Kim, R. Zboril, Noncovalent functionalization of graphene and graphene oxide for energy materials, biosensing, catalytic, and biomedical applications. Chem. Rev. **116**, 5464–5519 (2016)
129. Y. Suda, T. Ono, M. Akazawa, Y. Sakai, J. Tsujino, N. Homma, Preparation of carbon nanoparticles by plasma-assisted pulsed laser deposition method—Size and binding energy dependence on ambient gas pressure and plasma condition. Thin Solid Films **415**, 15–20 (2002)
130. Y.-P. Sun, B. Zhou, Y. Lin, W. Wang, K.A.S. Fernando, P. Pathak, M.J. Meziani, B.A. Harruff, X. Wang, H.F. Wang, P.J.G. Luo, H. Yang, M.E. Kose, B.L. Chen, L.M. Veca, S.-Y. Xie, Quantum-sized carbon dots for bright and colorful photoluminescence. J. Am. Chem. Soc. **128**, 7756–7757 (2006)
131. D. Pan, J. Zhang, Z. Li, M. Wu, Hydrothermal route for cutting graphene sheets into blue-luminescent graphene quantum dots. Adv. Mater. **22**, 734–738 (2010)

132. N. Dhenadhayalan, K.-C. Lin, R. Suresh, P. Ramamurthy, Unravelling the multiple emissive states in citric-acid-derived carbon dots. J. Phys. Chem. C **120**, 1252–1261 (2016)
133. L. Wang, S.-J. Zhu, H.-Y. Wang, S.-N. Qu, Y.-L. Zhang, J.-H. Zhang, Q.-D. Chen, H.-L. Xu, W. Han, B. Yang, H.-B. Sun, Common origin of green luminescence in carbon nanodots and graphene quantum dots. ACS Nano **8**, 2541–2547 (2014)
134. H. Ding, S.-B. Yu, J.-S. Wei, H.-M. Xiong, Full-color light-emitting carbon dots with a surface-state-controlled luminescence mechanism. ACS Nano **10**, 484–491 (2016)
135. X.M. Wen, P. Yu, Y.R. Toh, X.T. Hao, J. Tang, Intrinsic and extrinsic fluorescence in carbon nanodots: Ultrafast time-resolved fluorescence and carrier dynamics. Adv. Opt. Mater. **1**, 173–178 (2013)
136. S. Zhu, Y. Song, X. Zhao, J. Shao, J. Zhang, B. Yang, The photoluminescence mechanism in carbon dots (graphene quantum dots, carbon nanodots and polymer dots): Current state and future perspective. Nano Res. **8**, 355–381 (2015)
137. G. Yang, C. Wu, X. Luo, X. Liu, Y. Gao, P. Wu, C. Cai, S.S. Saavedra, Exploring the emissive states of heteroatom-doped graphene quantum dots. J. Phys. Chem. C **122**, 6483–6492 (2018)
138. M.E. Casida, T.A. Wesolowski, Generalization of the Kohn–Sham equations with constrained electron density formalism and its time-dependent response theory formulation. Int. J. Quantum Chem. **96**, 577 (2004)
139. T.A. Wesolowski, Hydrogen-bonding-induced shifts of the excitation energies in nucleic acid bases: An interplay between electrostatic and electron density overlap effects. J. Am. Chem. Soc. **126**, 11444 (2004)
140. J. Neugebauer, On the calculation of general response properties in subsystem density functional theory. J. Chem. Phys. **131**, 084104 (2009)
141. M.A. Sk, A. Ananthanarayanan, L. Huang, K.H. Lim, P. Chen, Revealing the tunable photoluminescence properties of graphene quantum dots. J. Mater. Chem. C **2**, 6954–6960 (2014)
142. S. Kim, S.W. Hwang, M.-K. Kim, D.Y. Shin, D.H. Shin, C.O. Kim, S.B. Yang, J.H. Park, E. Hwang, S.-H. Choi, G. Ko, S. Sim, C. Sone, H.J. Choi, S. Bae, B.H. Hong, Anomalous behaviors of visible luminescence from graphene quantum dots: Interplay between size and shape. ACS Nano **6**, 8203–8208 (2012)
143. S.H. Jin, D.H. Kim, G.H. Jun, S.H. Hong, S. Jeon, Tuning the photoluminescence of graphene quantum dots through the charge transfer effect of functional groups. ACS Nano **7**, 1239–1245 (2013)
144. B. Zhu, S. Sun, Y. Wang, S. Deng, G. Qian, M. Wang, A. Hu, Preparation of carbon nanodots from single chain polymeric nanoparticles and theoretical investigation of the photoluminescence mechanism. J. Mater. Chem. C **1**, 580–586 (2013)
145. K. Hola, A.B. Bourlinos, O. Kozak, K. Berka, K.M. Siskova, M. Havrdova, J. Tucek, K. Safarova, M. Otyepka, E.P. Giannelis, R. Zboril, Photoluminescence effects of graphitic core size and surface functional groups in carbon dots: COO^- induced red-shift emission. Carbon **70**, 279–286 (2014)
146. W. Kwon, S. Do, J.-H. Kim, M.S. Jeong, S.-W. Rhee, Control of photoluminescence of carbon nanodots via surface functionalization using para-substituted anilines. Sci. Rep. **5**, 12604 (2015)
147. K. Hola, M. Sudolska, S. Kalytchuk, D. Nachtigallova, A.L. Rogach, M. Otyepka, R. Zboril, Graphitic nitrogen triggers red fluorescence in carbon dots. ACS Nano **11**, 12402–12410 (2017)
148. Q. Xu, Y. Liu, R. Su, L. Cai, B. Li, Y. Zhang, L. Zhang, Y. Wang, Y. Wang, N. Li, X. Gong, Z. Gu, Y. Chen, Y. Tan, C. Dong, T.S. Sreeprasad, Highly fluorescent Zn-doped carbon dots as Fenton reaction-based bio-sensors: An integrative experimental–theoretical consideration. Nanoscale **8**, 17919–17927 (2016)
149. Y. Dong, J. Cai, X. You, Y. Chi, Sensing applications of luminescent carbon based dots. Analyst **140**, 7468–7486 (2015)
150. H. Sun, L. Wu, W. Wei, X. Qu, Recent advances in graphene quantum dots for sensing. Mater. Today **16**, 433–442 (2016)

151. H. Zhang, H. Zhang, A. Aldalbahi, X. Zuo, C. Fan, X. Mi, Fluorescent biosensors enabled by graphene and graphene oxide. Biosens. Bioelectron. **89**, 96–106 (2017)
152. A.P. Demchenko, M.O. Dekaliuk, Novel fluorescent carbonic nanomaterials for sensing and imaging. Methods Appl. Fluoresc. **1**, 042001 (2013)
153. S. Li, Y. Li, J. Cao, J. Zhu, L. Fan, X. Li, Sulfur-doped graphene quantum dots as a novel fluorescent probe for highly selective and sensitive detection of Fe^{3+}. Anal. Chem. **86**, 10201–10207 (2014)
154. X. Sun, Y. Wang, Y. Lei, Fluorescence based explosive detection: From mechanisms to sensory materials. Chem. Soc. Rev. **44**, 8019–8061 (2015)
155. B. Ju, Y. Wang, Y.-M. Zhang, T. Zhang, Z. Liu, M. Li, S.X.-A. Zhang, Photostable and low-toxic yellow-green carbon dots for highly selective detection of explosive 2,4,6-trinitrophenol based on the dual electron transfer mechanism. ACS Appl. Mater. Interfaces **10**, 13040–13047 (2018)